San Jose State University

SJSU ScholarWorks

7-2023

Extending the Service-Life of Bridges using Sustainable and Resilient Abutment Systems: An Experimental Approach to Electrochemical Characterization of Lightweight Mechanically Stabilized Earth

Fariborz M. Tehrani
California State University, Fresno

Kenneth L. Fishman
Mineta Transportation Institute

Farmehr M. Dehkordi
California State University, Fresno

Follow this and additional works at: https://scholarworks.sjsu.edu/mti_publications

Part of the Transportation Commons, and the Transportation Engineering Commons

SJSU SAN JOSÉ STATE UNIVERSITY

MTI MINETA TRANSPORTATION INSTITUTE

Extending the Service-Life of Bridges Using Sustainable and Resilient Abutment Systems: An Experimental Approach to the Electrochemical Characterization of Lightweight Mechanically Stabilized Earth

Fariborz M. Tehrani   Kenneth L. Fishman   Farmehr M. Dehkordi

CSUTC California State University Transportation Consortium

FRESNO STATE
Discovery. Diversity. Distinction.

Mineta Transportation Institute

Founded in 1991, the Mineta Transportation Institute (MTI), an organized research and training unit in partnership with the Lucas College and Graduate School of Business at San José State University (SJSU), increases mobility for all by improving the safety, efficiency, accessibility, and convenience of our nation's transportation system. Through research, education, workforce development, and technology transfer, we help create a connected world. MTI leads the Mineta Consortium for Transportation Mobility (MCTM) funded by the U.S. Department of Transportation and the California State University Transportation Consortium (CSUTC) funded by the State of California through Senate Bill 1. MTI focuses on three primary responsibilities:

Research

MTI conducts multi-disciplinary research focused on surface transportation that contributes to effective decision making. Research areas include: active transportation; planning and policy; security and counterterrorism; sustainable transportation and land use; transit and passenger rail; transportation engineering; transportation finance; transportation technology; and workforce and labor. MTI research publications undergo expert peer review to ensure the quality of the research.

Education and Workforce

To ensure the efficient movement of people and products, we must prepare a new cohort of transportation professionals who are ready to lead a more diverse, inclusive, and equitable transportation industry. To help achieve this, MTI sponsors a suite of workforce development and education opportunities. The Institute supports educational programs offered by the Lucas Graduate School of Business: a Master of Science in Transportation Management, plus graduate certificates that include High-Speed and Intercity Rail Management and Transportation Security Management. These flexible programs offer live online classes so that working transportation professionals can pursue an advanced degree regardless of their location.

Information and Technology Transfer

MTI utilizes a diverse array of dissemination methods and media to ensure research results reach those responsible for managing change. These methods include publication, seminars, workshops, websites, social media, webinars, and other technology transfer mechanisms. Additionally, MTI promotes the availability of completed research to professional organizations and works to integrate the research findings into the graduate education program. MTI's extensive collection of transportation-related publications is integrated into San José State University's world-class Martin Luther King, Jr. Library.

_____

Extending the Service-Life of Bridges Using Sustainable and Resilient Abutment Systems: An Experimental Approach to the Electrochemical Characterization of Lightweight Mechanically Stabilized Earth

Fariborz M. Tehrani, PhD, PE, ENV SP, PMP, SAP, F.ASCE

Kenneth L. Fishman, PhD, PE, M.ASCE

Farmehr M. Dehkordi, MSc, M.RILEM

July 2023

TECHNICAL REPORT DOCUMENTATION PAGE

1. Report No. 23-11	2. Government Accession No.	3. Recipient's Catalog No.
4. Title and Subtitle Extending the Service-Life of Bridges using Sustainable and Resilient Abutment Systems: An Experimental Approach to Electrochemical Characterization of Lightweight Mechanically Stabilized Earth		**5. Report Date** July 2023
		6. Performing Organization Code
7. Authors Fariborz M. Tehrani, https://orcid.org/0000–0002–7618–8009 Kenneth L. Fishman Farmehr M. Dehkordi		**8. Performing Organization Report** CA-MTI-2225
9. Performing Organization Name and Address Mineta Transportation Institute College of Business San José State University San José, CA 95192–0219		**10. Work Unit No.**
		11. Contract or Grant No. ZSB12017-SJAUX
12. Sponsoring Agency Name and Address State of California SB1 2017/2018 Trustees of the California State University Sponsored Programs Administration 401 Golden Shore, 5th Floor, Long Beach, CA 90802		**13. Type of Report and Period Covered**
		14. Sponsoring Agency Code
15. Supplemental Notes		

16. Abstract

Bridges are critical components of transportation infrastructure. This research addresses the need to extend the service life of bridges by improving the safety and reliability of bridge abutments and reducing their life-cycle cost and footprints. Mechanically stabilized earth (MSE) is a known strategy to enhance the economy and performance of bridge abutments. In addition, the application of rotary-kiln-manufactured lightweight aggregate backfills improves the performance of MSE bridge abutments with a leaner structural system. Such improvements include a reduction of structural demands due to a lower density, free drainage of granular materials, a high internal friction angle, less settlement with no consolidation, and accelerated construction requiring less compaction effort. This project aims to assess the electrochemical properties of expanded shale, clay, and slate (ESCS) aggregates and their influence on the corrosion of embedded steel strips. The experimental methodology involves evaluating current testing methods to measure electrical resistivity, pH, sulfate, chloride, and corrosion considering various gradation, moisture, dilution, and curing conditions. Samples represent available sources of ESCS with one source of normal weight aggregates for comparison. Results indicate the appropriateness of ESCS for addressing corrosion in MSE backfills. Further, outcomes provide guidelines to categorically predict the corrosivity of steel reinforcement when ESCS is employed as fill within MSE systems. These guidelines can help optimize the design and reduce the need to maintain and rehabilitate bridges, abutments, and approach and departure slabs on roadways to keep transportation systems safe and cost-efficient for sustainable infrastructure.

17. Key Words Corrosion, Lightweight aggregate, Mechanically stabilized earth, Bridge abutments, Electrical resistivity, pH, Sulfates, Chloride, Backfills	**18. Distribution Statement** No restrictions. This document is available to the public through The National Technical Information Service, Springfield, VA 22161.		
19. Security Classif. (of this report) Unclassified	**20. Security Classif. (of this page)** Unclassified	**21. No. of Pages** 97	**22. Price**

Form DOT F 1700.7 (8–72)

ACKNOWLEDGMENTS

CONTENTS

LIST OF FIGURES

LIST OF TABLES

Executive Summary

This project involves an experimental study of the application of rotary-kiln-manufactured lightweight aggregates in mechanically stabilized earth (MSE) bridge abutments. The motivation for this research stems from the need to extend the service life, reduce the life-cycle cost, and improve the safety and reliability of bridge abutments. Identifying and mitigating the corrosion of metal reinforcement in such applications is a means to extend the service life of bridges and reduce the need for the maintenance and rehabilitation of bridges, abutments, and approach and departure slabs on roadways.

The principal objective of this research project is to evaluate the current test methods and standards for assessing the corrosivity of expanded shale, clay, and slate (ESCS) aggregates compared to existing standards for normal-weight aggregates. For this purpose, the study included a series of electrical resistivity and chemical tests on selected materials with various particle sizes. Comparing results with current standards indicated the efficacy of the test and facilitated the development of a protocol for assessing the corrosion of embedded steel reinforcement in lightweight fills, including ESCS.

The application of rotary-kiln-manufactured lightweight aggregate backfills improves the performance of MSE bridge abutments with a leaner structural system. Such improvements include a reduction of structural demands due to a lower density, free drainage of granular materials, a high internal friction angle, less settlement with no consolidation, and accelerated construction requiring less compaction effort. This project aims to assess the electrochemical properties of ESCS aggregates and their effect on the corrosion of embedded steel strips.

The project's methodology involves evaluating current testing methods to measure electrical resistivity, pH, sulfate and chloride ion contents, and corrosion with respect to various gradations, moisture conditions, and sample preparations, including dilution ratios and curing conditions. Samples are representative of available ESCS sources and include one source of normal-weight aggregates. The test program consists of the following measurements:

- Physical characteristics (e.g., grain size, apparent specific gravity, bulk specific gravity, and absorption) per ASTM C136

- Electrical resistivity per AASTHO T 288, ASTM WK24621, ASTM G187, and Tex-129-M using Humboldt H-4385D Resistivity Meter

- The pH of the aqueous content per AASHTO T 289, ASTM D4972, NCHRP 21–06, and Tex-620-M using a Gilson Portable pH Meter MA-258

- Sulfate and chloride ion contents per AASHTO T 290 and T 291, and Tex-620-M using Hanna HI38001 Sulfate and HI3815 Chloride Test Kits

- Corrosion rates of steel coupons embedded in aggregate samples per ASTM G1 and G162 using Elcometer 456 and Gamry Reference 620 PotentioStat

Results

The results provide guidelines to categorically predict the corrosivity of steel reinforcement in ESCS backfills of MSE systems.

Physical Properties

Lightweight aggregates have 20% to 40% lower density and 500% to 600% higher water absorption than normal weight aggregates. Geotechnical blends from three sources had adequate fine portions and were suitable for testing in accordance with current AASHTO standards, whereby the samples are separated by the 2 mm (#10) sieve. Five other blends lacked the required portion passing the #10 sieve and therefore were tested in accordance with TxDOT, ASTM, and other standards that specified testing with as-is gradations. These samples represent coarse blends that are common materials for MSE backfills.

Electrical Resistivity

Coarse aggregates have a higher resistivity compared to passing 2 mm (#10) aggregates by a factor of up to 10 for the same sources of materials. Further, the drained condition of materials also increased the resistivity by a factor of 10. The 24-hour saturation practice in the corrosion tests shows some reduction as conductive contents find adequate time to disperse through the aqueous content. Trends observed between resistivity and grain size distribution parameters, including grading number (GN) and a fineness modulus (FM), confirm that resistivity measured via TX-129-M is typically higher than by AASHTO T 288. However, the results converge for higher GN and lower FM values.

pH

Comparing pH values obtained from the fine aggregate samples that passed the 2 mm (#10) sieve and tested in accordance with AASHTO T 289 with measurements via TX-620-M standards reveals that the testing method has an impact of approximately 2.1% on the measurements, but the difference for individual samples varies between 0.2 and 1.4, for which the latter difference is significant. Similar observations apply to results via ASTM D4972 with an overall 2.4% difference and the individual pH gap between 0.1 and 0.4, with one exception of a difference of 0.7. Data from this study also suggests that electrical resistivity tends to drop as the pH increases, but the low fidelity of suggested curves rejects a strong influence of pH on electrical resistivity.

Sulfate and Chloride

All observed trends suggest a reduced electrical resistivity for high sulfate and chloride content values. The declining trends of resistivity versus sulfate have a higher coefficient of determination than those for chloride, most likely due to high sulfate concentrations as opposed to chloride contents. With respect to chemical activity, sulfate contents vary between 0.56 and 37 mEq/kg (SO_4^{--} with a valence of 2 mEq/mmole and weight of 96 mg/mmole), and chloride contents vary between 0.021 and 4.6 mEq/kg (Cl^- with a valence of 1 mEq/mmole and weight of 35.5 mg/mmole).

Corrosion Rate

Results indicate that all coarse lightweight aggregate samples have lower corrosion rates than the coarse normal-weight aggregate samples. Further, the average corrosion rate from moist samples is considerably lower than that of wet samples. The difference is larger for coarse blends compared to fine samples, as fine samples keep more moisture after drainage and during air drying. Each wetting and drying cycle results in higher resistivity, lower sulfate and chloride ion contents, and lower corrosion rates, with some exceptions. Notably, the normal-weight sample has lower sulfate and chloride ion contents than most lightweight aggregates, which confirms prior observations of higher electrical resistivity. The coarse lightweight aggregate samples show lower corrosion rates compared to the normal-weight aggregates despite lower resistivity and higher salt contents.

Performance Analysis

The thresholds of sulfate and chloride contents before they have a significant effect on corrosion are 200 and 100 mg/kg, respectively. However, the low corrosivity of some samples does not support the adoption of these triggering values for ESCS fills. Thus, it may be appropriate to raise these thresholds to 500 mg/kg for sulfate and 150 mg/kg for chlorides considering the performance of ESCS aggregates.

Conclusions

The study described in this report investigated the electrochemical properties of eight sources of ESCS lightweight aggregates. Samples included a combination of fine- and coarse-blended aggregates compared with fine and coarse normal-weight aggregate samples. The gradations, densities, and water absorptions of each sample were evaluated using ASTM standards. Electrochemical tests included electrical resistivity, pH, and sulfate and chloride ion contents of aggregates in various moisture conditions according to AASHTO, TxDOT, and ASTM following NASEM (2021). These tests were partially verified through third-party testing by a certified laboratory.

Further, corrosion studies were conducted on aggregate samples during wetting, saturation, drainage, and air-drying cycles at 7, 14, 28, 90, 182, and 364 days. This report covers the first

28 days of testing, to be followed with amendments covering the complete cycle. Interpreting corrosion measurements involved comparisons and correlations with measurements of the resistivity of the aggregates in the test box and resistivity/conductivity, pH, and the sulfate and chloride ion contents of aqueous extracts.

Electrochemical tests indicated a significant gap between the properties of coarse and fine aggregates and, therefore, showed that TxDOT standards are more applicable to coarse-blended aggregates when used as geotechnical fills. The corrosion tests revealed that the corrosivity of galvanized and carbon steel coupons in lightweight fills does not exceed those of normal-weight aggregates despite having lower resistivity or higher sulfate ion contents. Hence, we suggest revised limits for electrochemical properties to current industry guidelines, such as AASHTO for the expected corrosion rates of lightweight aggregates used as fill-in geotechnical engineering applications to allow higher electrical resistivity and sulfate and chloride contents.

Implementation

Corrosivity and corresponding metal loss models are input to the service life analysis for MSE walls, a significant parameter in lifecycle cost analysis. In addition, a bottom-up approach to energy and emissions results in environmental product declarations for the complete product of an MSE abutment. The product's lifecycle begins with mining the raw materials and manufacturing in the production plant and extends to transportation at the site and construction of bridge abutments. The lifecycle analysis ends with the project's decommissioning and the reuse and recycling of products.

Further, the adequate thickness of steel bars in MSE systems indicates the available strength and rigidity of MSE bridge abutments. These characteristics contribute to abutment performance, their interaction with approach and departure slabs, and their potential settlement. Information about the remaining cross-section and strength of reinforcements during service can serve as input to structural analyses to examine the system's robustness and the vulnerabilities to extreme loadings and natural disasters such as earthquakes. These characteristics provide an objective measure of the resilience of bridge systems.

1. Introduction

1.1 Motivation and Objectives

The motivation for this research stems from the need to extend the service life, reduce the life cycle cost, and improve the safety and reliability of bridge abutments. This project endeavors to develop advanced solutions for applying rotary-kiln-manufactured lightweight aggregates in mechanically stabilized earth (MSE) bridge abutments (Figure 1). Identifying and mitigating the corrosion of metal reinforcement in such a solution is a means to extending the service life of bridges and to reducing the need to maintain and rehabilitate bridges, abutments, and approach and departure slabs on roadways. This solution identifies cost-effective MSE systems for the long-term service life of roads and bridges. The outcome of this project reduces the lifecycle cost, input energy, and greenhouse gas emissions associated with the construction, maintenance, and rehabilitation of MSE bridge abutments and other backfills involving embedded steel products.

This project's innovative approach is the evolution of current testing methods to measure the corrosion of reinforcing steel elements as a function of the electrochemical properties of backfill materials. This project extends and amends current national efforts led by the National Cooperative Highway Research Program (NCHRP), the American Association of State Highway and Transportation Officials (AASHTO), and several Departments of Transportation (DOT), including Texas's and California's, highlighting past achievements in Fresno and new possibilities for the State of California.

Figure 1. Schematic View of Bridge Components with MSE Abutments (Red)
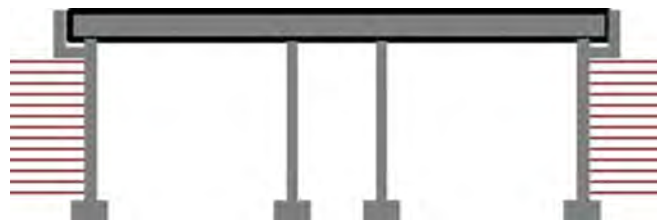
1.2 Synopsis

The principal objective of this research project is to evaluate the current testing methods to assess the corrosivity of expanded shale, clay, and slate lightweight aggregates compared to existing standards for normal-weight aggregates. For this purpose, the experimental efforts included a series of electrical resistivity and chemical tests on selected materials with various particle sizes. Comparing results with current standards indicated the test's efficacy.

1.3 Background

The corrosion of metallic materials, such as steel strips or grids, inside MSE walls is an essential concern that limits their designed service life and increases their maintenance and repair costs.

Current practice recognizes resistivity as a strong indicator of the corrosivity of backfill materials (Snapp 2012). However, the existing standards, i.e., AASHTO T 288 and other relevant AASHTO standards, apply to materials with a significant fine component (Vilda 2009). Thus, DOTs, such as the Texas DOT, have attempted to revise these standards and propose adjustments (Brady, Parsons, and Han 2016; Castillo et al. 2014; IDOT 2021; Petrasic 2008; Salazar 2010). At the same time, the application of alternative materials, such as lightweight ESCSs in North America, Europe, and Asia, has gained popularity due to their lightness, ease of compaction, sustainability, and durability. Application of ESCS contributes to enhancing drainage and corrosion reduction compared with on-site materials. Experimental shake table studies of lightweight backfills have indicated the significance of low density, a high internal friction angle, and high damping for the high performance of MSE systems (Munjy et al. 2014; Sadrinezhad, Tehrani, and Jeevanlal 2019; Tehrani et al. 2018; Xiao, Tehrani and Zoghi 2013). Figure 2 highlights the following characteristics of the ESCS (dark red shades) as opposed to conventional materials (dark gray shades) within a matrix of performance measures (cost, time, energy, emissions) and lifecycle phases from mining to reuse (Tehrani 2023b):

- Less Demand: ESCS reduces the dead load and the soil-bearing pressure

- Less Fill: reduction of the self-weight reduces the sliding force and required foundation length to provide resistance

- Leaner System: a combination of reduced density and higher internal friction angle reduces the active pressure requiring a thinner wall or less reinforcement

- Less Settlement: lower density and higher stability reduce soil settlement and backfill volume changes

- Fast and Easy Placement and Reuse: ESCS requires fewer compaction efforts and provides full recyclability

- Less Lane Closure: ease of compaction contributes to accelerated construction and required lane closures

- Free Drainage: granular composition of ESCS facilitates free drainage and reduces the need for supplemental drainage systems

Corrosivity relations determine the service life of MSE walls, a significant parameter in lifecycle cost assessment (LCA). In addition, a bottom-up approach to energy and emissions results in environmental product declarations (EPD) for the complete product of an MSE abutment. The development of the EPD requires a comprehensive understanding of the infrastructure's service life and associated footprints to facilitate the decision-making process for planners and designers to achieve sustainability goals. Hence, the LCA is a prerequisite for the EPD. The product's lifecycle begins with mining raw materials and manufacturing in the production plant and extends

to transportation at the site and construction of bridge abutments. The lifecycle analysis ends with the decommissioning of the project and the reuse and recycling of products (Tehrani 2023a).

Further, adequate thickness of steel bars in MSE systems indicates the available strength and rigidity of the bridge abutment and provides evidence of the potential settlement of approach and departure slabs. Therefore, a structural analysis examines the robustness of the system and vulnerabilities to extreme loadings and natural disasters such as earthquakes. These characteristics provide an objective measure of the resilience of bridge systems (Tehrani 2022).

Figure 2. Schematic Illustration of Lightweight Aggregate Benefits in MSE Applications (Tehrani 2023)
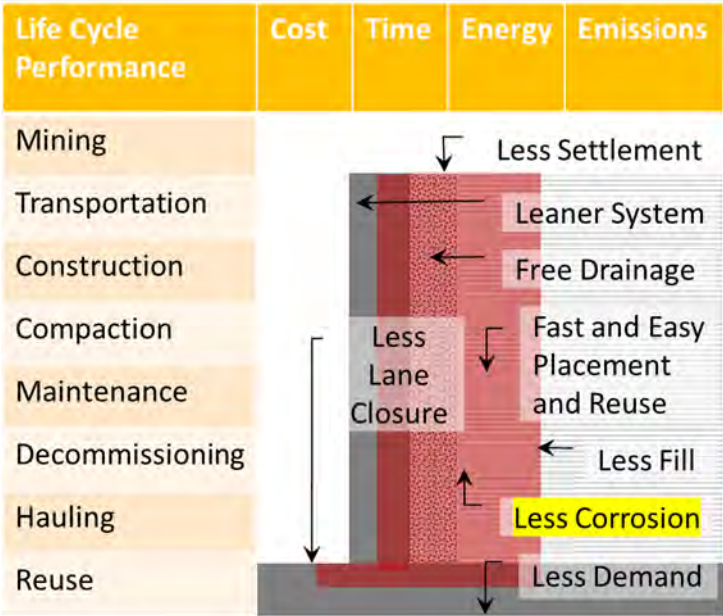
In addition, Figure 3 displays the observed difference in NASEM (2021) between normal-weight and lightweight aggregates concerning corrosion rate and resistivity (Tehrani 2021). While the low-corrosion rate in this figure is not unique to lightweight aggregates, the low number of lightweight specimens in the referenced study warrants additional investigations. Therefore, there is a need to assess the efficiency of current practices and to propose adjustments for these alternative aggregates with respect to testing standards and the interpretation of results (NASEM 2020; NASEM 2021).

Figure 3. Difference Between ESCS and Mineral Aggregates Concerning Corrosion Rate and Resistivity (Tehrani 2021, Courtesy of ESCSI)

Data Source: NASEM 2021
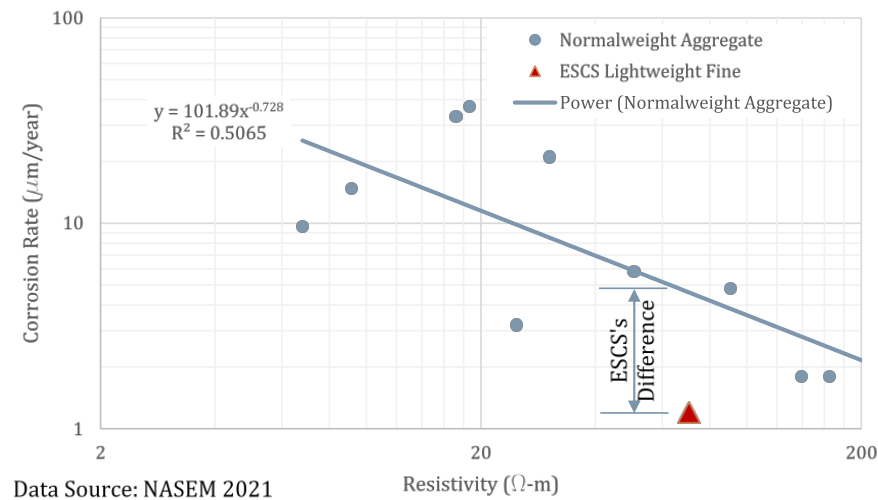
This report highlights the application of rotary-kiln-manufactured (Figure 4) ESCS aggregates (Figure 5) available worldwide (Figure 6). The production process, shown in Figure 4, is nearly identical worldwide, and the difference between aggregate properties is related to the raw materials being shale, clay, or slate. Hence, the variation of the physical and mechanical properties of these manufactured aggregates tends to be less than those extracted from mines or recycled sources, or industrial byproducts that do not experience quality control processes typical of a manufacturing plant (Holm and Ries 2007).

Figure 4. A Rotary-kiln Manufacturing Plant of Expanded Aggregates (Courtesy of Norlite)

The visual characteristics of rotary-kiln-manufactured lightweight aggregates, such as color, shape, and size, may differ for various sources, as shown in Figure 5. The post-production screening processes provide customized products with different characteristics, such as shape and size, for specific applications. However, physical and mechanical properties such as porosity, absorption, density, and strength are similar. The identical chemistry of vitrified aggregates and their porous microstructure achieved in the rotary kiln is responsible for the homogeneity of such properties across products from different manufacturers (Tehrani 1998).

Figure 5. Sample Expanded Shale with Coarse, Medium, and Fine Gradations from
Left to Right

The selection of lightweight aggregates from participating producers, shown in Figure 6, requires two essential criteria. First, the selection should include aggregates expanded from all three sources: shale, clay, and slate. Second, the selection should consider materials from different domestic regions, representing variations in the raw materials. Hence, results would apply to projects located in various locations within reach of any specific producer.

Figure 6. ESCSI Production Plants (Courtesy of ESCSI)
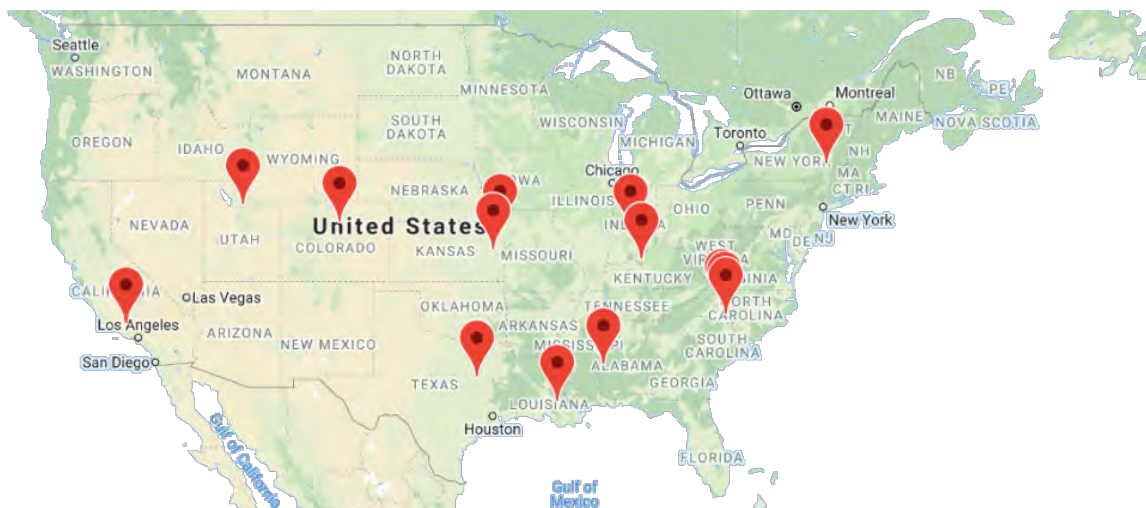
2. Literature Review

2.1 Characteristics of Mechanically Stabilized Earth Systems

Among different earth-retaining structures, the mechanically stabilized earth wall system is an economic system utilized in various applications worldwide, generally known as MSE walls. This technology was created in France in the 1960s, and a decade later, the Federal Highway Administration (FHWA) brought it to North America. The quick construction process, tolerance for a larger settlement, economic aspects, and superior aesthetics over traditional cast-in-place concrete structures increased the rate of the built walls from a few dozen a year to more than 600 per year after 1990 (Holz, Christopher, and Berg 1998; Anderson, Gladstone, and Sankey 2012).

A typical section of an MSE wall includes a reinforced body, reinforcing members, and facing elements (Figure 7). The reinforced body may consist of conventional earth, such as normal-weight fills; and lightweight aggregates, such as expanded shale, clay, and slate. Reinforcing members are available in a wide range of strips, grids, and textiles. Facing elements protect the wall face from raveling and provide the connection point for reinforcing members. The overall performance of the MSE system is the direct result of the mechanical, physical, and chemical interaction between these components. The pull-out strength of reinforcing members is a function of the friction and cohesion between the reinforced body and the reinforcing member and provides the wall's strength and internal stability. Similarly, the degradation of reinforcing members, such as the corrosion of steel straps inside reinforced earth, determines the wall's durability and service life and eventually degrades the mechanical capacity of the system (Beben 2015; Jack and Wilmott 2011).

Figure 7 A Schematic View of An MSE Wall Section
(Harpstead, Schmidt, and Christopher 2010)
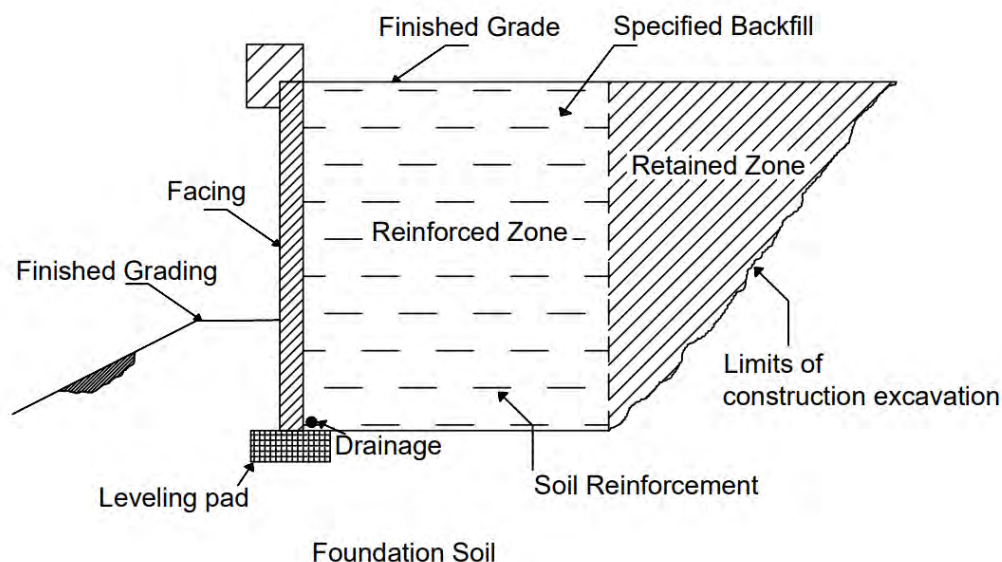
Various environmental conditions such as seawater, rain, humidity, and temperature influence the corrosion process, that is, the oxidization or loss of electrons. However, the corrosion of metallic surfaces does not always result in the degradation of the metallic materials. For instance, oxidized copper forms a green-colored layer that protects subsurface copper from exposure to corrosive agents. In contrast, oxidized iron, known as rust, lacks adherence to the subsurface and therefore is vulnerable to scaling and progressively exposing subsurface metallic contents to oxidization. Figure 8 demonstrates this process for steel reinforcement embedded in the soil, where the electric current potential within the soil environment relates to the corrosion rate through coating thickness, passivity, and pitting tendency (Revie 2008).

Figure 8. Corrosion of Steel in Contact with Soil (Kolay, Tajhya, and Mondal 2020)
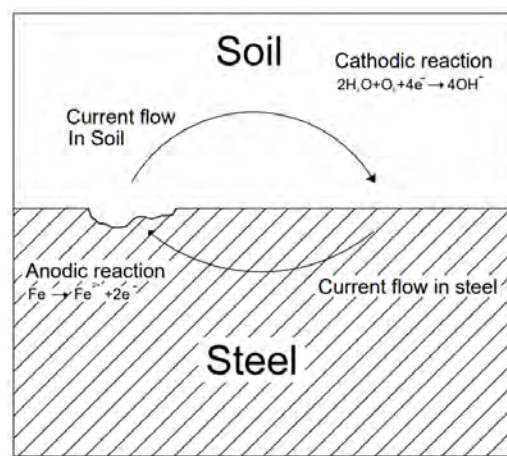
The presence of water in a typical backfill and the penetration of corrosive ions or their existence in the soil facilitates the current flow of electrons within the resulting electrolyte and ultimately causes corrosion (Elias et al. 2009). Inherent variations in the soil's compaction, composition, and moisture exacerbate these effects by creating localized anodes and cathodes at the surface of metallic elements, making embedded steel straps in backfills susceptible to corrosion (Jack and Wilmott 2011). In this process, an electrical current flows from the anode to the cathode in the soil. This flow is reversed in steel from the cathode to the anode. Therefore, rust and iron oxides are created in the places where iron is oxidized. An accumulation of rust relates to decreased steel sections and the reduced strength and stiffness of reinforcing elements (Darwin, Mindess, and Young 2003). The corrosion rate and availability of steel reinforcement determine the MSE system's service life (Snapp 2015). These relations have warranted studies on backfill characteristics' influence of on the corrosion of MSE steel reinforcement. These features involve pH, electrical resistivity, and the concentration of soluble salts such as sulfate and chloride (Arciniega et al. 2019).

2.2 Electrochemical Properties of Backfills

Electrical resistivity

Resistivity is a measure of the impedance of an electrical current. The corrosiveness of the soil can be predicted by measuring the minimum soil resistivity (Elias 1990; Elias et al. 2009; NASEM 2011; Padilla, Ghods, and Alfantazi 2013). Soil resistivity measurements can be made in situ or on a laboratory bench. According to Ohm's Law, resistance (R) equals the ratio of induced voltage (V) to current (I) in comparable units.

$$R = \frac{V}{I}$$

In theory, passing an electric current through a block of soil produces a voltage that can be measured and used to determine resistance. According to the block's geometry, resistance (R) in Ω is transformed to resistivity (ρ) in Ω.cm, which is then expressed as a property of the soil and the length (L) and cross-section area (A) of the soil box (Samouëlian et al. 2005).

$$\rho = R\frac{A}{L}$$

Materials and solutions with high resistivity have low ion concentrations and poor electron transport. Low-resistivity materials have large ion concentrations and are excellent electron conductors. Resistance is related to pH because basic and acidic pH values favor more ions in a solution, which lowers resistivity. The presence of water reduces the resistivity of soil, as water is highly conductive and allows electrons to flow more rapidly from the metal reinforcement. This process, also known as wet corrosion, is possible at low temperatures, as opposed to dry corrosion, which is only possible at high temperatures. Therefore, soil resistance at ambient temperature and moisture are instrumental in assessing corrosion potential. The American Association of State Highway and Transportation Officials (AASHTO) requires a minimum resistivity of 3,000 Ω.cm to ensure that structural backfill are not aggressively corrosive (Elias 1990; Thapalia et al. 2011). Various DOTs recognize values between 2,000 to 5,000 Ω.cm as the minimum resistivity following variations of the AASHTO T288 or ASTM G187 standards (Elias 1990). The NCHRP 20–50 Report (NCHRP 1978) suggests a list of limits for soil's aggressiveness as a function of electrical resistivity (Table 1). The AASHTO standard method to determine minimum resistivity requires testing wet fine materials in a slurry state, which does not necessarily resemble the actual state of the soil. Arciniega et al. (2018) indicate that particle size distribution influences soil resistivity. Hence, the testing sample for determining electrical resistivity should resemble the placed backfill concerning gradation and moisture, which is not necessarily a slurry state (McCarter 1984).

Table 1. Effects of Soil Corrosion and Resistivity (after NCHRP 1978)

Aggressiveness	Resistivity (Ω.cm)
Very Corrosive	< 700
Corrosive	700 to 2,000
Moderately Corrosive	2,000 to 5,000
Mildly Corrosive	5,000 to 10,000
Non-Corrosive	> 10,000

Recent studies have highlighted the relationship between laboratory assessments and field observations concerning corrosion (Adkins and Rutkowski 1997; Brady, Parsons, and Han 2016). Typical parametric studies have involved solid, liquid, and voids in the soil and employed non- or semi-destructive methods such as electrical resistivity (ER), half-cell potential (HCP), and galvanostatic pulse measurement (GPM) as indicators of the corrosion rate. More advanced electrochemical techniques, such as Linear Polarization Resistance (LPR) or Tafel extrapolation, are also available to estimate the corrosion rate of the reinforcement with greater accuracy. The LPR and Tafel techniques apply a current to reinforced steel to estimate its corrosion rate via electron loss flow (Samouëlian et al. 2005).

pH

The pH of the soil represents hydrogen activity in the soil mixture and can determine how the soil will affect the corrosion of any metal reinforcement buried in the ground. High corrosion rates are related to severely acidic soils, with a pH of less than 4, or strongly alkaline soils, with a pH greater than 10. Hence, a typically recommended range for pH to minimize corrosion damage is from 5 to 10. The amount of dissolved salts in the soil is one of the main elements that affect its pH level; high salt content will result in higher pH levels in the soil. AASHTO T289 and ASTM G51 are common methods to measure pH (Elias et al. 2009).

Sulfates and chlorides

Chlorine catalyzes metallic corrosion by dissolving the protective passive oxide layers on the metal surface (Broomfield 2003; Bertolini et al. 2013). Sulfate reduction produces a substantial amount of acid, most frequently by sulfate-reducing bacteria (SRB), which causes pitting corrosion. Because of these factors, many state DOTs have restricted the soluble chlorine and sulfate levels in materials used for MSE walls. However, many rocks contain small amounts of sulfide minerals such as pyrite (FeS_2). The reduced form of sulfur is sulfide, which can oxidize in aerobic environments to generate sulfate (SO_4^{2-}), linked to acid production (i.e., the release of H^+):

$$F_e S_2 + (7/2)O_2 + H_2O \rightarrow F_e^{2+} + 2SO_4^{2-} + H^+$$

$$F_e S_2 + 14F_e^{3+} + 8H_2O \rightarrow 15F_e^{2+} + 2SO_4^{2-} + 16H^+$$
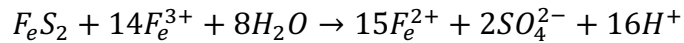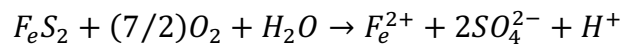
Sulfate and H⁺ ions can impact corrosion rates. To maintain oxidative weathering via the Fe(III) pathway, Fe(II) must be oxidized to regenerate Fe(III) according to the following reaction:

$$F_e^{2+} + (1/4)O_2 + H^+ \rightarrow F_e^{3+} + (1/2)H_2O$$
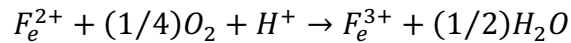
Salts like chlorides, and sulfates increase the electrolytic conductivity of soil solutions as more salts in the soil result in more electrons lost from metallic reinforcement due to the electrochemical process of corrosion. The typical maximum allowable level of salt content for chlorides is 100 ppm and for sulfates it is 200 ppm (Elias et al. 2009).

Steel reinforcements are particularly susceptible to localized corrosion (pitting corrosion) caused by chloride anions (Cl⁻). High concentrations of chlorides (such as sodium chloride, NaCl) accelerate the corrosion of embedded steel members. Sources of chloride might be deicing salts, often known as antifreeze, applied on roads to lower the freezing point of water or seawater, which have a salt content of 3.5% by weight. This salt content disassociates into free ions (including Cl⁻) in water and moves with the water into the system's pores. Chloride ions travel to the reinforcing steel level from the surrounding media and damage the passive layer of protection on the steel surface when enough Cl⁻ reaches the steel surface. Hence, one of the crucial parameters to evaluate the corrosion initiation time is the chloride content (Elias et al. 2009).

Techniques for measuring sulfates in soil extracts involve turbidimetry, atomic absorption spectrophotometry, inductively coupled plasma spectroscopy (ICP), potentiometry, or high-performance liquid chromatography. The preferred method depends on the amount of sample, the chemical constituents of the extract, the available instrumentation, and the concentration of sulfate in the extracts. The turbidimetric method produces satisfactory results in samples containing high sulfate levels (e.g., acidic subsoils and mine soil extracts). Ion chromatography and High-Performance Liquid Chromatography (HPLC) with conductivity detectors are capable instruments for determining low sulfate concentrations in soil extracts. These procedures are advantageous when measuring nitrate, chloride, fluoride, and sulfate at the same time. However, measuring sulfate using HPLC alone can be time-consuming and costly because the soil extracts must be filter-sterilized.

Johnson and Nishita's (1952) procedure is the most sensitive and accurate colorimetric method for determining sulfate. However, because this method involves reducing sulfate to sulfide and then measuring the sulfide by colorimetry, it is time-consuming and highly dependent on operator skill. Sulfide generated by the Johnson and Nishita (1952) procedure can also be measured electrochemically using a sulfide-specific electrode. For electrochemical measurements, sulfate is reduced using the Johnson and Nishita procedure, then adsorbed onto a sulfide anti-oxidant buffer;

the sulfide activity is measured using a sulfide electrode. This electrochemical measurement is also time-consuming and requires the analyst to pay close attention to detail (Elias et al. 2009).

There are some standard methods to measure sulfate and chloride, including AASHTO T290 and T291, ASTM D4327, and their variations adopted by other jurisdictions. The maximum sulfate and chloride values to avoid corrosion damage are 100 and 200 ppm, respectively. However, these numbers change based on the specified methods in each jurisdiction (Elias et al. 2009).

Soil moisture

Darbin, Jailloux, and Montuelle (1988) noted that the highest corrosion rates occur between 60% and 85% of moisture saturation levels. Elias et al. (2009) investigated fourteen active California sites, revealing that most backfills had more than 65% saturation levels. As a result, it is crucial to evaluate the effect of moisture levels in MSE wall backfill on the corrosion of embedded steel reinforcement. The soil moisture controls the properties of the soil-metal interface, electrical conductivity, and ionic migration in soils, which all directly affect the corrosion processes (Azoor et al. 2019). Accordingly, the corrosion of the embedded metallic reinforcement at dry conditions is negligible. Studies have highlighted the possibility of an optimal moisture level to maximize the corrosion rate. This optimal level relies on the interaction between electrical conductivity and oxygen diffusion (Stott and John 2010). Therefore, the funicular state of moisture in soil causes more corrosion damage to ferrous materials than the pendular state. This observation is significant as fine soil particles such as clay tend to have higher saturation levels than coarse particles such as silt or sand (Marot, Bendahmane, and Nguyen 2012).

2.3 Electrochemical Corrosion of Steel

Corrosion of galvanized steel

The expected service life of the MSE wall determines the basis for assessing corrosion damage and specifying acceptable backfill properties. In this project's approach, the remaining thickness of steel reinforcement at the end of service life, for instance after 75 or 100 years, benchmarks the performance of the MSE system. The difference between the nominal thickness of steel reinforcement at construction and the remaining thickness at the end of service life is the sacrificial thickness of metal (AASHTO 2017). Protective materials may include epoxy-coated, galvanized, or stainless steel. Galvanized steel is a typical example of a sacrificial layer to protect carbon steel, as opposed to stainless steel, which changes steel's chemical composition by adding chromium. Galvanization involves adding a layer of zinc using hot dip galvanizing or electro-galvanizing. The latter, known as cold galvanizing, is an electrolysis-based process using a mixture of saline and zinc to obtain a thin zinc coat (Porter 1994).

The classification of elements and alloys based on their electrochemical scale indicates their relative corrosion potential and tendency to corrode. A higher corrosion potential means more energy is needed to lose electrons, which inhibits corrosion. The contact of two materials, such as zinc and

steel, with different corrosion potentials forms a galvanic cell. The metal with the lower corrosion potential, in this case zinc, will act as an anode, ready to be consumed by corrosion, whereas the metal with the higher corrosion potential, in this case carbon steel, acts as a cathode that is protected from corrosion (Asgari, Toroghinejad, and Golozar 2009). Hence, zinc physically acts as a barrier between the steel surface and soil moisture and chemically acts as a sacrificial anode. When exposed to a corrosive environment, the zinc coating corrodes, forming a thin zinc-oxide film. Thus, the corrosion rate of zinc reduces with exposure time (Padilla and Alfantazi 2013). AASHTO presents a model with an initial thickness of 86 mm of zinc coating to be corroded at a rate of 15 mm/year in the first two years and 4 mm/year afterward until the zinc coat is lost in 16 years. Then, the corrosion of carbon steel begins at 12 mm/year for the remainder of the 75-year service life and results in 708 mm loss per side of the steel (AASHTO 2017; NASEM 2011).

Corrosion damages

The primary corrosion process of embedded steel in MSE backfills involves the loss of carbon steel ions, as an electrolyte, to soil moisture (Elias et al. 2009). In galvanized steel, zinc is sacrificed to postpone the corrosion of core carbon steel (Davis 2000). Pitting corrosion may also occur as a localized process when a small area of the anodic metal is exposed to the high demand of electrons by the large cathodic region (Chen, Bronson, and Knittel 1985; Szklarska-Smialowska 1986; Knittel and Bronson 1984). Iron corrosion forms an oxyhydroxide passive coating, which is vulnerable to chloride ions and results in pits on the surface (Jones 1996). The progress of galvanized steel corrosion depends on the corrosiveness of the soil media and the thickness of the exposed zinc. The stress of the reinforcing steel may also influence the corrosion of exposed steel after the deterioration of the protective zinc layer (Fontana and Greene 1986).

Laboratory and field studies may detect corrosion damages using various passive and active techniques (RILEM Technical Committee 2010; Zaki et al. 2015). Monitoring zinc dissolution typically indicates the soundness of the galvanized steel throughout time. Electrochemical impedance spectroscopy may also reveal the influence of chloride ions on zinc, steel, and their interface. Further, a standard polarization scan can determine the resistance of galvanized steel to corrosion. In addition, several techniques are available to monitor the in-situ corrosion rate of steel reinforcement embedded in an existing MSE wall, including probes to detect resistivity, moisture, and temperature and metallic coupons to assess the corrosiveness of the soil media (Blitz and Simpson 1996).

3. Methodology

The methodology involves evaluating current testing methods to measure electrical resistivity, pH, sulfate and chloride ion contents, and corrosion with respect to various gradations, moisture conditions, and sample preparations, including dilution ratios and curing conditions. Testing standards consist of currently accepted professional practice and industry methods, including proposed and implemented procedures following local, national, and international modifications.

Gradations are varied to include those with significant portions passing 2 mm (#10), which are suitable for testing according to current AASHTO standards and those that include material passing 9.5 mm (3/8") for pH measurement (as described in NCHRP 21–06) and as-is gradations that are often used in construction. The gradations of specimens subject to corrosion testing were blends intended for geotechnical applications produced by each manufacturer.

Specimens include one sample of normal weight aggregates for comparison and obtained from local sources in California (Sakrete) and eight samples of lightweight expanded shale, clay, and slate aggregates from selected ESCS producers, as shown in Figure 9, including Arcosa Lightweight (expanded clay from Frazier Park, California and expanded shale from Livingston, Alabama; Shepherdsville, Kentucky; and Streetman, Texas), Buildex (expanded shale from Dearborn, Missouri), Carolina Stalite Company (expanded slate from Gold Hill, North Carolina), Holcim Utelite (expanded shale from Coalville, Utah), and Norlite (expanded shale from Cohoes, New York). The testing apparatus's dimensions and configurations were adjusted and modified to accommodate large-size aggregates and render conclusions on size effect using small and large box sizes. The comparison between testing results using current and proposed sample sizes and methods of preparation for various sources of ESCS and normal weight aggregates facilitates the development of the proposed specifications for the testing and evaluation of ESCS samples.

Figure 9. Selected Shipped Materials from Producers in Sealed Plastic Buckets or Bags

The test program includes the following measurements:

- Physical characteristics (e.g., grain size, apparent specific gravity, bulk specific gravity, and absorption)

- Electrical resistivity

- The pH of the aqueous content

- Sulfate and chloride ion contents

- The corrosion rate of steel coupons embedded in aggregate samples

3.1 Physical Characteristics

Aggregates were received in sealed bags to preserve the samples (Figure 10). The sieve analysis follows ASTM C136 to differentiate coarse and fine aggregates (Figure 11). The results contribute to selecting appropriate test methods and sample preparation for electrochemical testing. The percentage of the sample passing the 4.75 mm (#4) sieve is used to identify samples as coarse or fine. Results for blended samples represent a weight-based average of coarse and fine aggregates. Bulk, relative, and apparent density measurements follow ASTM C29, C127, and C128 (Figures 12 and 13).

Figure 10. Selected Samples Stored in Sealed Bags

Figure 11. Standard Test for the Sieve Analysis of Coarse Samples (ASTM C136)

Figure 12. Standard Test for the Specific Gravity of Fine Samples (ASTM C128)

Figure 13. Standard Test for the Bulk Density of Samples (ASTM C127)

3.2 Electrical Resistivity

Specimens were placed and saturated in a clear plastic box, and then subjected to electrical resistivity measurements. Specimens were tested for resistivity per AASHTO T 288 and optional methods per ASTM WK24621, ASTM G187, and Tex-129-E modified by Tex-129-M for small and large box sizes (Table 1). The AASHTO T 288 requires preparing fine materials passing the 2 mm (#10) sieve and does not allow the crushing of coarse aggregates to achieve the target gradation. Hence, this test does not apply to coarse aggregates or even fine aggregates passing the 4.75 mm (#4) sieve per ASTM C33/C33M or C330/C330M. The various sizes of materials were included in other tests to draw a comparison between results and assess the effect of the box size and the particle size for the proposed test. For this purpose, fine samples passing the 2 mm (#10) sieve were tested using AASHTO T 288 and Tex-129-M methods.

Furthermore, the saturation and drainage states differ between various testing procedures. Except for ASTM WK24621, which incorporates the drained condition, other tests mandate that the lowest resistivity measurement be achieved by adding water. The drained state simulates the situation of a free-draining backfill following water intrusion/infiltration, e.g., following a storm event. The saturated condition is least likely to be the case for free-draining coarse aggregates, such as those placed using ESCS.

Further, AASHTO T 288 differs from ASTM and TxDOT standards as it would allow a sample to be tested beyond saturation until it is a poorly mixed slurry. ASTM and TxDOT permit water to fill all internal pores of the aggregates and external voids between aggregates within the volume of the chosen box. However, the AASHTO standard requires the aggregates to be mixed with a virtually indefinite amount of water outside the box and then placed in the box for testing until achieving the least resistivity. Reported T 288 results in this report reflect such a slurry state. This mixing process typically results in a slurry of fine materials with water replacing solid particles. Although the liquefaction of fine particles is possible, this does not realistically represent the conditions of MSE backfills. Therefore, the application of Tex-129-M addresses the departure of testing criteria from realistic conditions.

Moreover, the length of time that a sample is soaked or cured after adding moisture is a test parameter that varies between zero and 24 hours per existing standards. Notably, the saturation of lightweight aggregates typically requires 72 hours of soaking instead of 24 hours for normal-weight aggregates. However, 72 hours of soaking is not realistic for backfilling materials. This fact implies that lightweight aggregates continue to absorb water when drainage begins after a hypothetical 24-hour soaking period, most likely caused by slow drainage.

Table 2. Resistivity Tests (NASEM 2020)

Standard	Grading	Moisture	Curing
AASHTO T 288	2 mm (#10)	Increments	12 h for the first increment
ASTM WK2461	None	Drained from a saturated condition	Soak for 24 h before draining
ASTM G187	6 mm (¼")	As-is for saturated	None
Tex-129-M	None	Increments, but saturated for coarse materials	None

The Humboldt H-4385D Resistivity Meter (Figure 14) was used to measure resistivity between $0.01\,\Omega$ to $10\text{M}\,\Omega$ with specified accuracies of 1.6% and 5% for ranges below and above $1\text{M}\,\Omega$, respectively. The temperature of the mixture was measured during the test using a Precision Digital Stem Thermometer with a range of -50 ℃ to 330 ℃ (-58 ℉ to 626 ℉) and an accuracy of 0.4 ℃ (0.8 ℉). In this manner, resistivity measurements could be corrected for temperature.

Figure 14. Humboldt H-4385D Resistivity Meter

Standard soil boxes for this meter are available at 75 mL and 280 mL volumes. In addition, Tex-129-M introduces small, medium, and large box dimensions for coarse aggregates. WK2461 also provides specific guidelines for selecting the box dimensions, including height and volume, as a function of the maximum aggregate size (Figure 15). Trends in Figure 16 were adopted to customize box dimensions for various aggregate sizes.

Figure 15. Selected Soil Boxes for the Electrical Resistivity Test

Figure 16. General Trends for the Minimum Dimensions of the Electrical Resistivity Box
(WK2461)
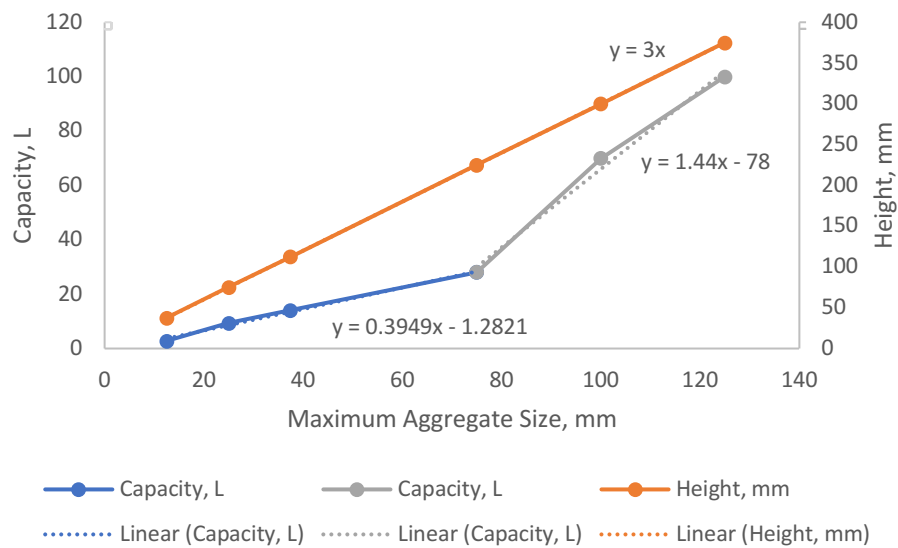
3.3 pH

Testing for pH follows AASHTO T 289 and optional methods per ASTM D4972, NCHRP 21–06, and Tex-620-E modified by Tex-620-M (Table 3). Specimens were diluted at specified ratios and mixed as recommended in each standard, and pH was measured using a Gilson Portable pH Meter MA-258 (Figure 17). The meter ranges from zero to fourteen pH, has a resolution of 0.01 pH, and an accuracy of 0.05 pH. The meter compensates pH for temperatures between 0 ˚C to 99.0 ˚C (32.0 ˚F to 210.2 ˚F).

Figure 17. The pH Meter and a Sample Solution

Like the electrical resistivity testing standards, existing AASHTO and ASTM standards apply to samples that have been separated by the 2 mm (#10) sieve. Hence, the proposed NCHRP 21–06 and TxDOT standards aim to address the need for the testing of coarse aggregates. Moreover, the pH test is characteristically sensitive to dilution, stirring, and stand time as primary parameters controlling the results. These parameters practically control the stability of the aqueous solution at the time of exposure to the pH probe. A magnetic stirrer was used to manage the mixing process over long periods. Furthermore, higher water content also ensures the availability of the aqueous solution for adequate submergence of the pH probe in highly absorbing materials such as lightweight aggregates.

Table 3. pH Tests (NASEM 2020)

Standard	Air Dry	Grading	Dilution[1]	Mixture	Stand Time
AASHTO T 289	Yes	2 mm (#10)	1:1	Stir every 15 min for 1 h	None
ASTM D4972	Yes	2 mm (#10)	1:1	Mix thoroughly	1 h
ASTM D8262	Yes	None	1:5	Stir for two min	24 h
NCHRP 21–06	No	9.5 mm (3/8")	1:1	Stirred	30 min
TX-620-M	Yes	None	1:10	Mixed for 30 min, stand for 1 h	None

[1] Solid: H_2O by weight

3.4 Sulfate and Chloride

Testing for sulfate and chloride contents followed AASHTO T 290 and T 291 and optional methods per Tex-620-J modified by Tex-620-M (Table 4). Specimens were diluted at specified ratios, mixed, and filtered as recommended. TxDOT criteria were the same for pH testing, but the AASHTO standard has a different dilution rate. Regardless, results were reported in mg/kg to account for varied dilution rates, that is, the measured concentration of the diluted sample (mg/L) is multiplied by the dilution ratio to get the proportion of weight in mg/kg in terms of the chloride's or sulfate's weight divided by the dry weight of the soil specimen. Specimens were centrifuged using a benchtop electric centrifuge machine with timer and speed control and filtered using 0.45 micrometer (Grade 42) qualitative filter paper or nylon syringe filters, as needed to ensure consistency of preparation procedures for all samples. A magnetic stirrer controlled stirring quality and standing time over long periods.

Table 4. Sulfate and Chloride Tests (after NASEM 2020)

Standard	Grading	Dilution[1]	Mixture	Filtration
AASHTO T 290	#10	1:3	Shaken, stand for 1 h	Centrifuge & Filter
AASHTO T 291	#10	1:3	Shaken for 20-sec, stand for 1 h, shaken	Centrifuge & Filter
TX-620-M	None	1:10	Mixed for 30 minutes, stand for 1 h	Filtered

[1] Solid: H_2O by weight

The testing apparatus includes Hanna HI38001 Sulfate (Figure 18) and HI3815 Chloride (Figure 19) Test Kits, and Hanna HI97751 Sulfate (Figure 20) and HI96753 Chloride Photometers (Figure 21). Chemical test kits have a range of 100 to 10,000 mg/L, a resolution of 10 mg/L, and an accuracy of 50 mg/L for sulfate; and a range of 0 to 1000 mg/L, a resolution of 1 mg/L, and an accuracy of 5 mg/L for chloride. Photometers have a range of 0 to 150 mg/L, a resolution of 1 mg/L, and an accuracy of 5 mg/L for sulfate; and a range of 0 to 20 mg/L, a resolution of 0.1 mg/L, and an accuracy of 0.5 mg/L for chloride. Considering available resolutions and accuracies, reported results are based on photometer outputs as verified by testing kits.

Figure 18. Sulfate Testing Kit Reagents

Figure 19. Chloride Testing Kit Reagents

Figure 20. Sulfate Photometers and Reagent

Figure 21. Chloride Photometers and Reagents

3.5 Corrosion Rate

The corrosivity of materials was tested using embedded galvanized and carbon steel coupons inside the proposed aggregates following ASTM G1 and ASTM G162 (Table 5). Coupons were 76 x 12.7 x 1.6 mm (3" × 1/2" × 1/16") standard coupons by Pacific Sensor with a 4.8 mm (3/16") diameter hole (Figure 22). Aggregate samples were soaked in deionized water for 24 hours and drained to air dry until the next soaking period. Examination periods were set for 1, 14, 28, 91, 156, and 364 days. The corrosion of steel coupons was assessed when exposed to ambient temperature and humidity outside the laboratory in Southern California. An Elcometer 456 was used to observe the loss of zinc coating from the surface over time, and a standard scale measured weight loss. This report covers the first 28 days of testing, to be followed with amendments covering the whole-year cycle (Figure 23).

Table 5. Corrosion Rate and Associated Tests

Measure	Grading	Preparation and Maintenance
Corrosion Rate and Electrical Resistivity of the Aggregate Box	As-is	Soaked for 24 h, drained, air dried for one week, repeated at 14, 28, 91, and 364 days.
Electrical Resistivity and pH of the Aqueous Solution	None	None
Sulfate and Chloride Content of the Aqueous Solution	None	Filtered

Figure 22. Testing Galvanized (Top) and Carbon (Bottom) Steel Coupons

Figure 23. Elcometer 456

A Gamry Reference 620 PotentioStat measured the corrosion rates periodically using the DC Corrosion tests with a graphite counter electrode and a copper sulfate reference electrode (Figure 24). Figures 25 and 26 show the typical arrangement of elements and their connectivity during corrosion tests. A customized plexiglass frame fixes the 38 mm (1.5") spacing between steel working electrodes and the graphite counter electrode. The top plexiglass plate provides an alternative reference electrode location for testing either coupon. A piece of 3M dielectric tape masks each connector to reduce noise. At each interval, the corrosion rate, electrical resistivity, pH, sulfate, and chloride contents were measured before and after soaking, draining, and air drying until the next consecutive saturation period. At the end of the periodic investigations, after one year, the Tafel slopes and corrosion rate will be observed from Tafel plot corrosion measurements, which require scanning over a broader range of overpotentials compared to linear polarization resistance (LPR) testing. An addendum to this report will cover those results.

Figure 24. Gamry Reference 620 PotentioStat and Software Interface

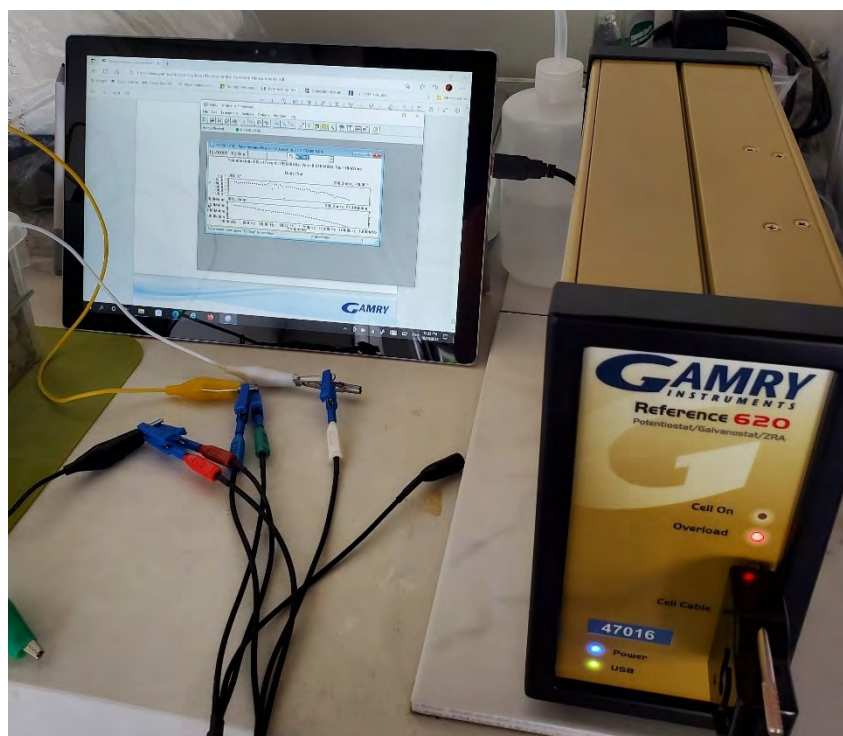Figure 25. Arrangement of Galvanized (Yellow Connector) and Carbon (Blue Connector) Steel Coupons as Working Electrodes and Reference Counter Electrode (Black Connector) Before Burial into Aggregate Samples

Figure 26. Connectivity During Corrosion Tests: Alternative Working Electrodes in Yellow and Green, Counter Electrode in Black at the Center, Reference Electrode in White, Resistivity Meter in Red and Black at the Edges

4. Results

4.1 Physical Properties

Figures 27 and 28 present the sieve analysis and density results for samples of lightweight aggregates (LW) from eight numbered sources and two samples of normal-weight aggregates (NW) for comparison. Two primary sets of aggregates include coarse and fine aggregates noted by C and F, respectively. Coarse and fine samples for each identifier are from the same source when available. Samples LW2, LW5, and LW8 were the only blended aggregates provided in one gradation. Specific grades for each test, such as particles passing a 2 mm (#10) sieve, were obtained from original samples as needed. Table 6 shows a summary of measured properties.

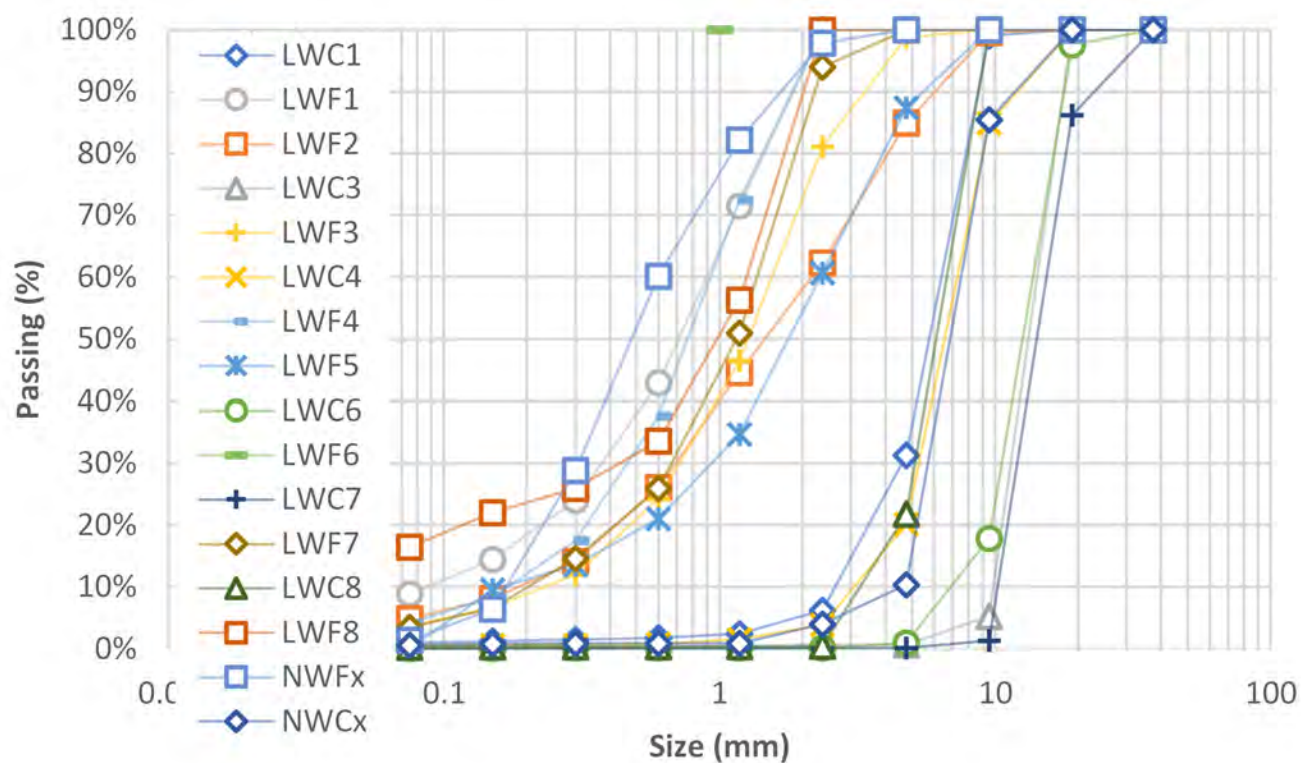Figure 27. Sieve Analysis of Sample Aggregates

Figure 28. Density of Sample Aggregates
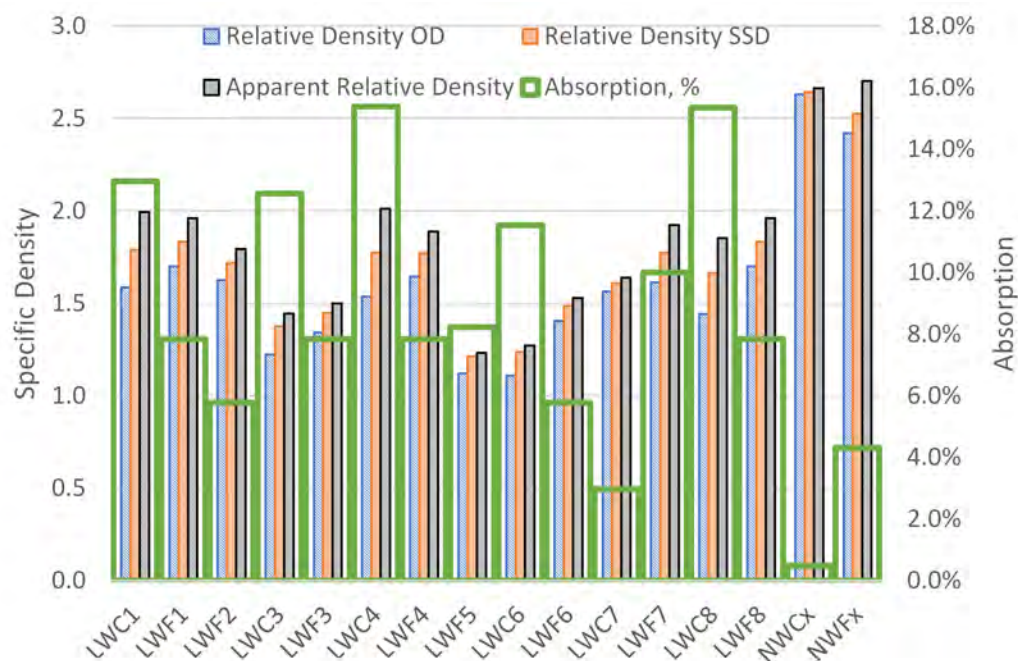
Table 6. Summary of Relative Densities

Aggregate	Lightweight	Normal weight
Relative Density	1.12–1.83	2.53–2.63
Relative Density, SSD	1.21–1.96	2.53–2.66
Apparent Density	1.23–2.01	2.66–2.7
Absorption, %	3.0–15.4	0.5–4.3

Figure 29 shows the general tendency of density measures to decrease for higher absorption rates of aggregates. These trends indicate that the absorption rate influences the relative density of LW due to porosity in the solid particles. The correlation provides the best fit for the oven-dried (OD) density measurements which appear to be most affected by absorption.

Figure 29. Density-absorption Trends of Sample Aggregates
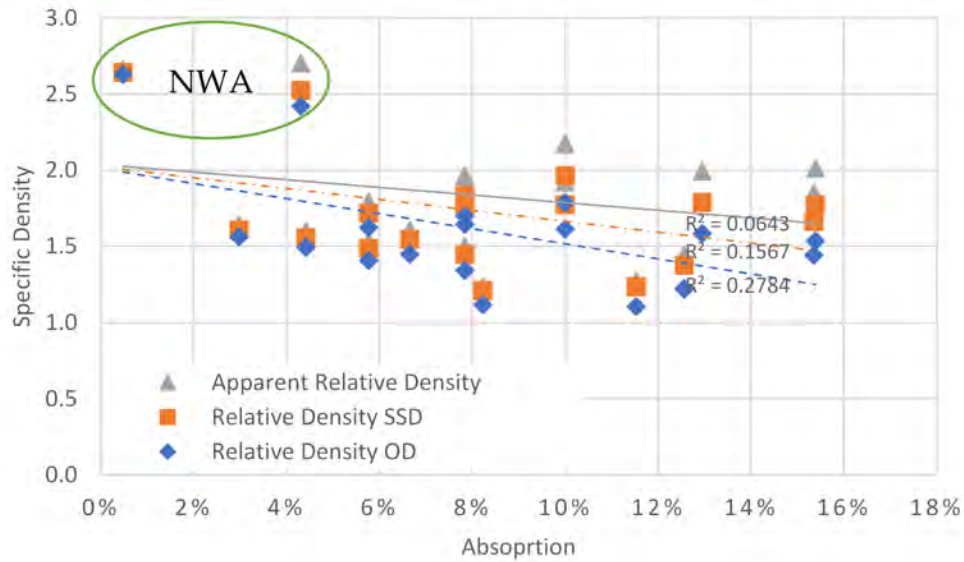
Figure 30 demonstrates the size distribution of sample aggregates. In this figure, gravel includes particles retained on the 6.3 mm (1/4") sieve, coarse sand includes particles passing the 6.3 mm (1/4") sieve and retained on the 0.425 mm (#40) sieve, fine sand includes particles passing the 0.425 mm (#40) sieve and retained on the 0.075 mm (#200) sieve, and fines includes particles passing the 0.075 mm (#200) sieve. Coarse samples in this figure do not have a fine sand component, and fine samples have less than 10% gravel.

Figure 30. Size Distribution of Sample Aggregates

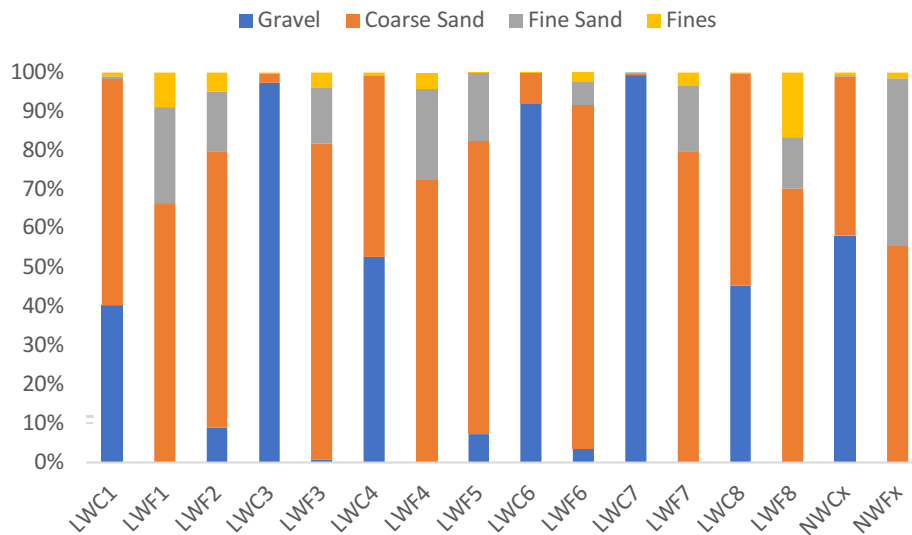Figure 31 utilizes the grading number (GN) and the fineness modulus (FM) as common standards in practice to quantify each sample based on coarseness or fineness parameters. GN is the sum of cumulative passing percentages from 25 mm (1"), 19 mm (3/4"), 9.5 mm (3/8"), 4.75 mm (#4), 2 mm (#10), 0.425 mm (#40), and 0.075 mm (#200) sieves. GN ranges between 1 and 7, with higher values corresponding to the finer materials. Coarse samples in this study have a GN of less than 3.2. The FM is the sum of cumulative retained percentages on 4.75 mm (#4), 2.36 mm (#8), 1.18 mm (#16), 0.600 mm (#30), 0.300 mm (#50), and 0.150 mm (#100) sieves. In this study, fine samples have an FM of less than 4. Figure 32 shows a schematic relationship between grading number and fineness modulus.

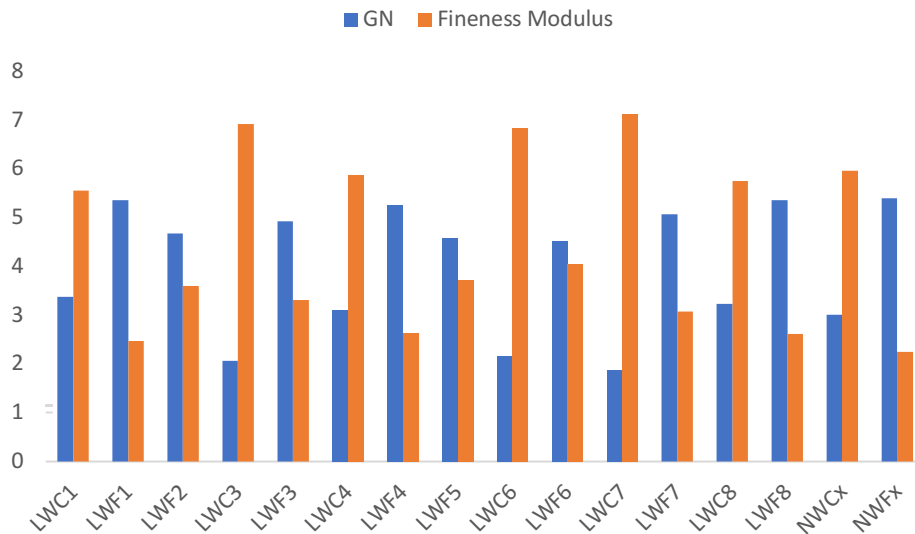Figure 31. Grading Number and Fineness Modulus of Sample Aggregates

Figure 32. Relationship Between Grading Number and Fineness Modulus of Sample Aggregates
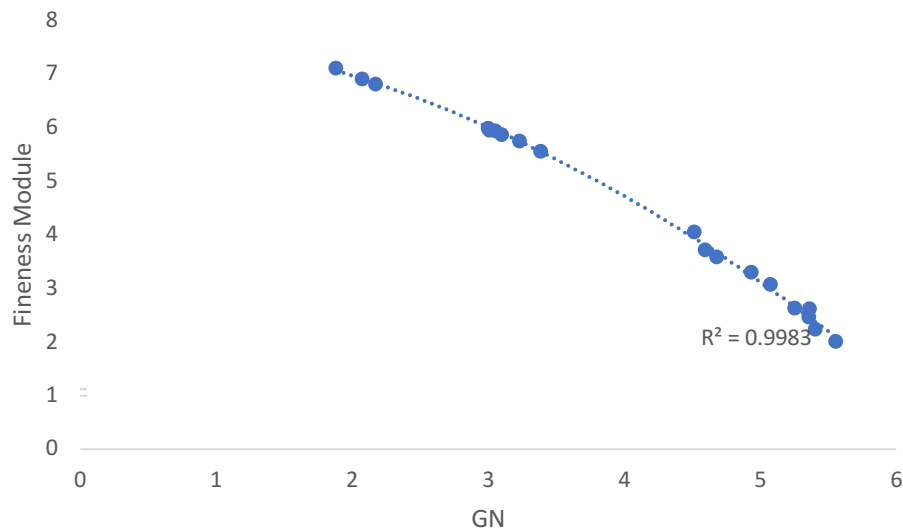
Figure 33 shows the passing percentage for the 2 mm (#10) sieve, which is the sole parameter in AASHTO standards to determine the appropriateness of testing standards for electrical resistivity, pH, and sulfate and chloride contents. Figure 34 shows the number of samples with certain percentages of samples passing the 2 mm (#10) sieve. Geotechnical blends from LW2, LW5, and NW sources, marked as LWF2, LWF5, and NWFx, had an adequate portion to qualify for AASHTO standards. Other blends, marked as LWC1, LWC3, LWC4, LWC6, LWC7, LWC8, and NWCx, lacked the required portion and, therefore, qualified for TxDOT, ASTM, and other tests that allowed as-is gradations. These samples represent coarse blends that are common materials for MSE backfills. For comparison, a special fine gradation was obtained from coarse blended materials labeled LWF1, LWF3, LWF4, LWF6, LWF7, and LWF8 to allow tests using AASHTO standards. Further, all fine blends, marked with F, were tested using TxDOT standards. Overall, more than half (9 out of 16) of the aggregate samples had at least 25% passing the 2 mm (#10) sieve.

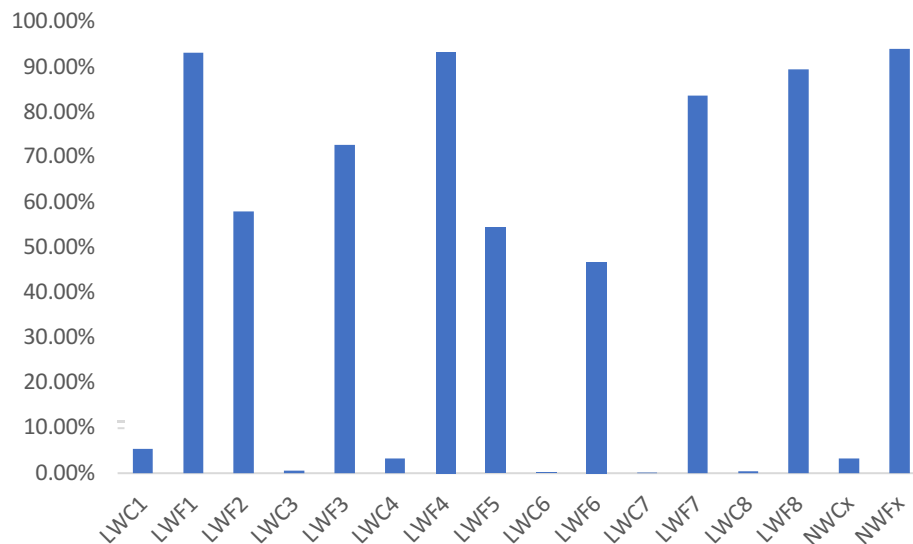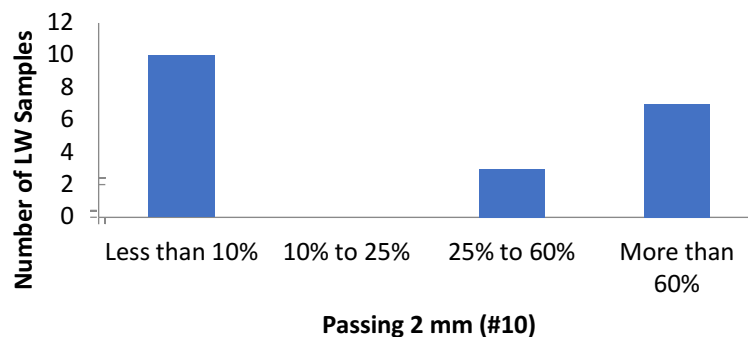Figure 33. Passing Percentage of 2 mm (#10) Sieve

Figure 34. Histogram of Passing 2 mm (#10) Sieve for Lightweight Aggregate Samples

4.2 Electrical Resistivity

Figure 35 shows the electrical resistance of sample aggregates using various standard methods and the results obtained after 24-hour soaking as part of the corrosion tests, also listed in Table 7. Due to the large variety of results, this figure benefits from a logarithmic scale. For each sample, T 288 tests apply to fine portions passing the 2 mm (#10) sieve, and 129-M, G187, and 24-hr. saturated tests apply to coarse blends according to each standard. Producers provided a separate fine sample for testing purposes only, even though such fine gradation was not included in the geotechnical blend for coarse samples that lacked an adequate portion of fine materials.

The AASHTO T 288 standard applies to materials with a significant content finer than 2 mm (#10) and is typically available for two box sizes of 75- and 280-ml volumes. The test was repeated using the 787 ml box size that fit the TX-129-M standard. It is apparent from this figure that coarse aggregates have a higher resistivity compared to fine aggregates by a factor of up to 10 for the same sources of materials. Furthermore, the drained condition of materials also increased the resistivity by a factor of 10, as shown by the 129-M Dr 787 data. The 24-hour saturation practice in the corrosion tests shows some reduction as conductive contents find adequate time to disperse through the aqueous content.

The results include the verification of the AASHTO T 288 tests performed by a certified laboratory, Cooper Testing Laboratory. These third-party verification results follow California Test 643, such as AASHTO tests. A significant difference between the AASHTO method and other methods, such as ASTM and California Tests, is the absence of adjustments for temperature. Due to the trivial need for such adjustments, the temperature adjustment is applied to all tests, including AASHTO. Figure 36 depicts data on the precision of the test results based on third-party verifications.

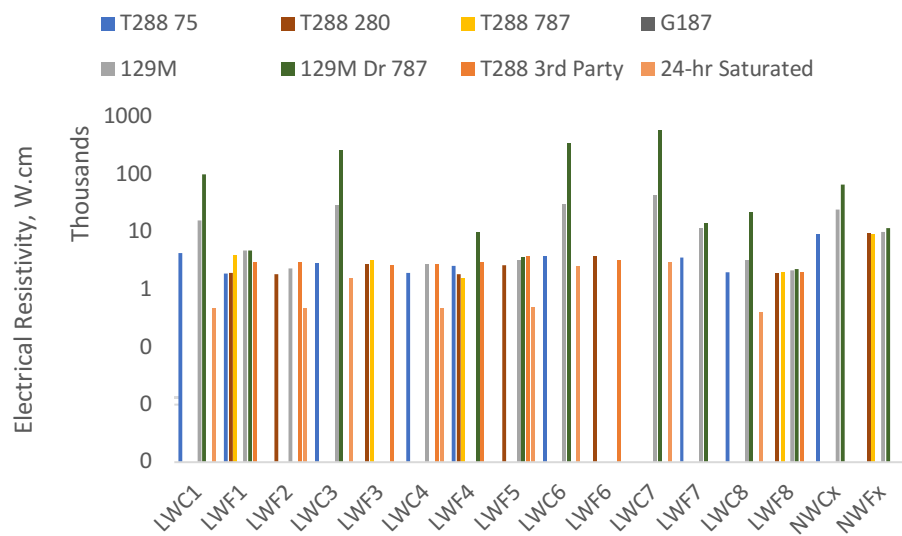Figure 35. Electrical Resistivity Results Using Standard Methods

Figure 36. Comparison of Electrical Resistivity Results with the Third-Party Verification Results
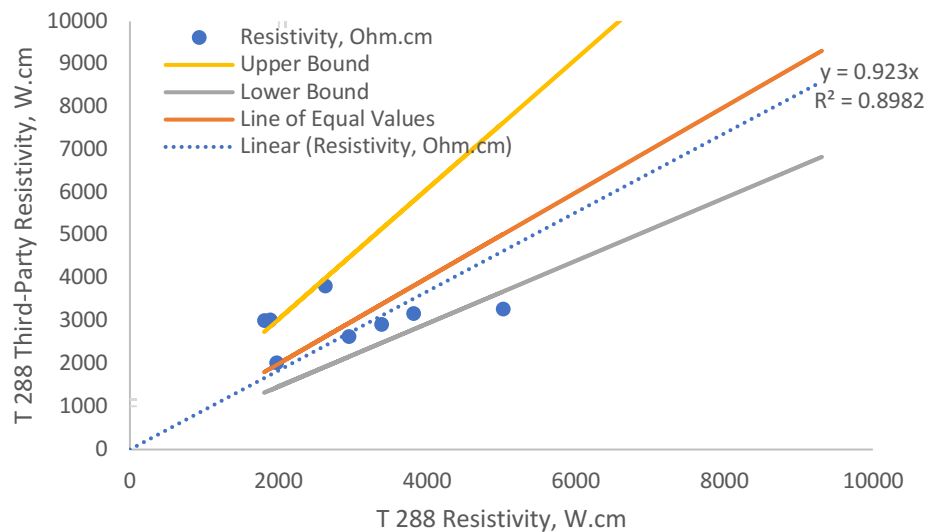
Table 7. Summary of Resistivity Test Results (Ω.cm)

	T 288 75-ml	T 288 280-ml	T 288 787-ml	G 187	129-M	129-M Dr 787-ml	T 288 third party	24-h saturated
LWC1					16,133	101,138		7,455
LWF1	4,296	1,983	3,870		4,770	4,851	2,919	
LWF2	1,924	1,852			2,346		3,036	3,031
LWC3					29,050	260,375		20,204
LWF3	2,862	2,771	3,197				2,646	
LWC4					2,715		2,819	2,845
LWF4	1,982	1,882	1,557			10,117	3,023	
LWF5	2,615	2,646			3,259	3,584	3,828	3,640
LWC6					30,385	354,259		19,302
LWF6	3,785	3,848					3,173	
LWC7				181,374	43,244	599,852		22,084
LWF7	3,608	3,553	7,901		11,461	14,364	3,290	
LWC8					3,264	21,603		
LWF8	2,008	1,922	1,986		2,154	2,277	2,025	2,533
NWCx					24,812	67,467		
NWFx	9,184	9,695	9,054		9,990	11,804		18,975

The TX-129-M applies to all sizes and requires a larger box size with a 787 ml volume for coarse materials. For comparison purposes, results include the AASHTO T 288 test result using the 787 ml box for the passing 2 mm (#10) particles. Figure 37 shows that the box size has a small influence on the recorded electrical resistance of fine materials. In contrast, the change in the testing method from AASHTO T 288 to TX-129-M, which removes the standing time, increases the recorded electrical resistivity for the same coarse aggregate size, as shown in Figure 38. In this figure, four samples with 20% or more passing the 4.75 mm (#4 sieve) have comparable resistivities measured from T 288 and 129-M tests. Their T 288 resistivity is below 2630 Ω.cm. However, other samples with negligible fine particles show a large gap between these results. Figure 39 shows the decline of the gap with the rise of fines, passing the 4.75 mm (#4) sieve in LW samples.

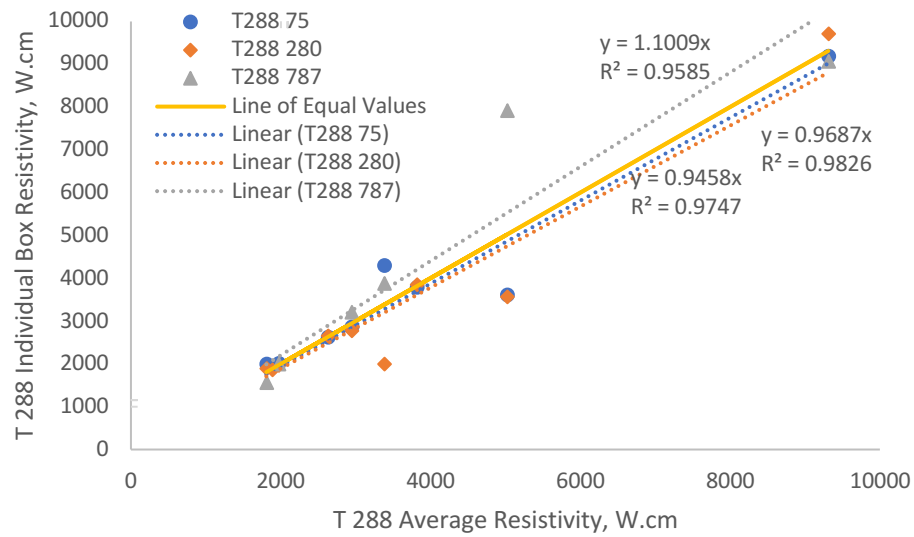Figure 37. Comparing Electrical Resistivity for Various Box Sizes

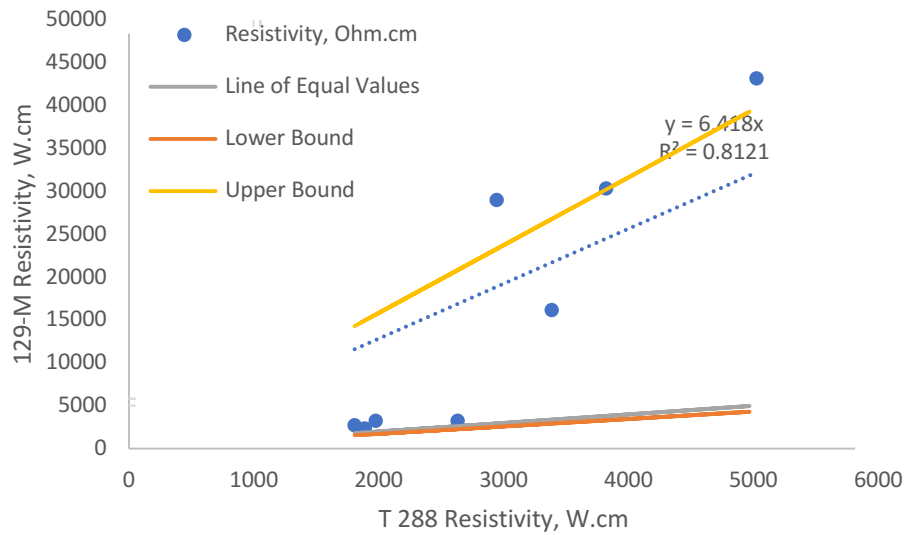Figure 38. Comparing Electrical Resistivity of Fine and Coarse Materials

Figure 39. Comparing Electrical Resistivity of Fine and Coarse Materials
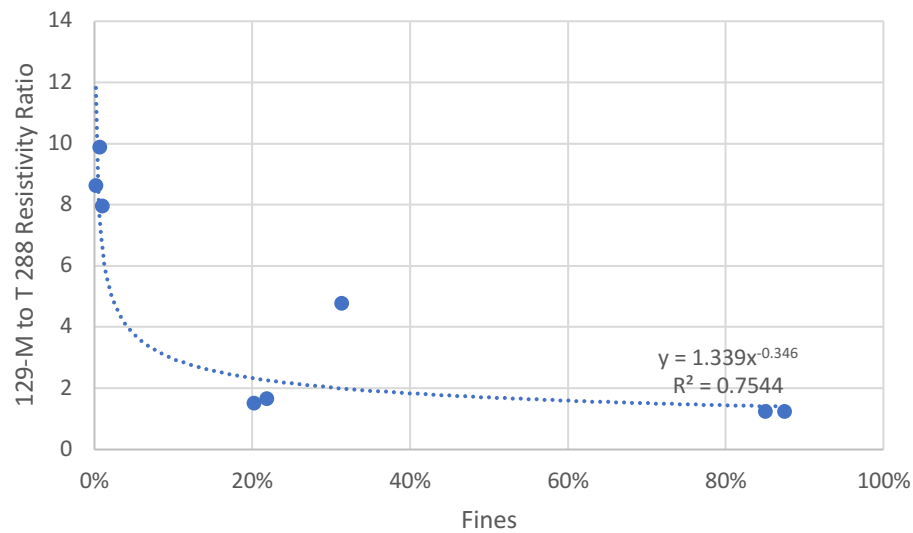
Figure 40 highlights a significant factor in the recorded electrical resistivity of aggregates where drained aggregates exhibit up to nearly 13 times higher values than submerged aggregates. This difference is higher for coarse aggregates than fine aggregates. It appears that fine materials are not free draining like coarse aggregates and retain water even after the drainage valve is opened. This process is due to capillarity at their high surface-to-volume ratios. Hence, their moist condition properties are more like wet conditions than coarse aggregates that show different properties under moist and wet conditions.

Figure 40. Comparing Electrical Resistivity of Saturated and Drained Conditions
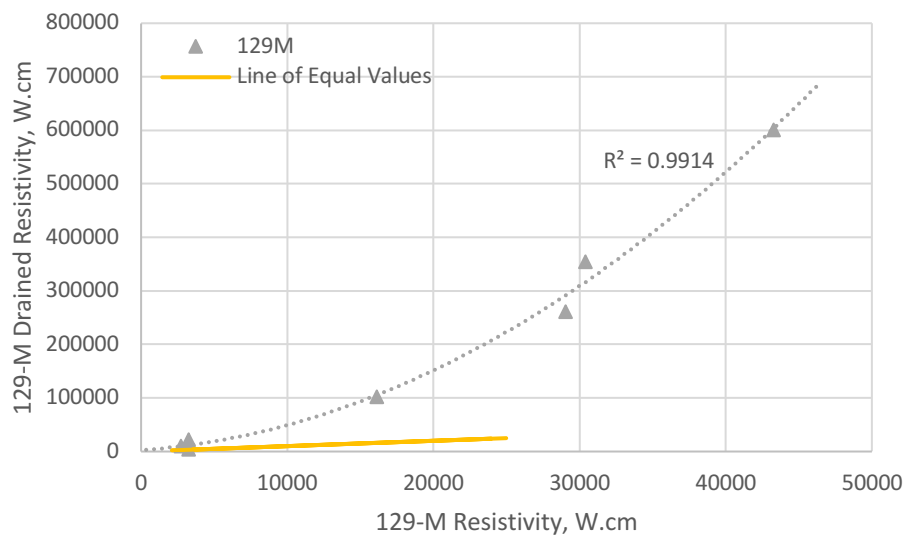
Figures 41 and 42 demonstrate potential trends between resistivity and size distribution parameters of grading number (GN) and fineness modulus. These trends confirm that TX-620-M results are typically higher than AASHTO T 288 results but may converge for higher GN values. For coarse samples without adequate fines, producers provided passing 2 mm (#10) particles for comparative testing purposes only, even though such gradations were not included in the geotechnical blend.

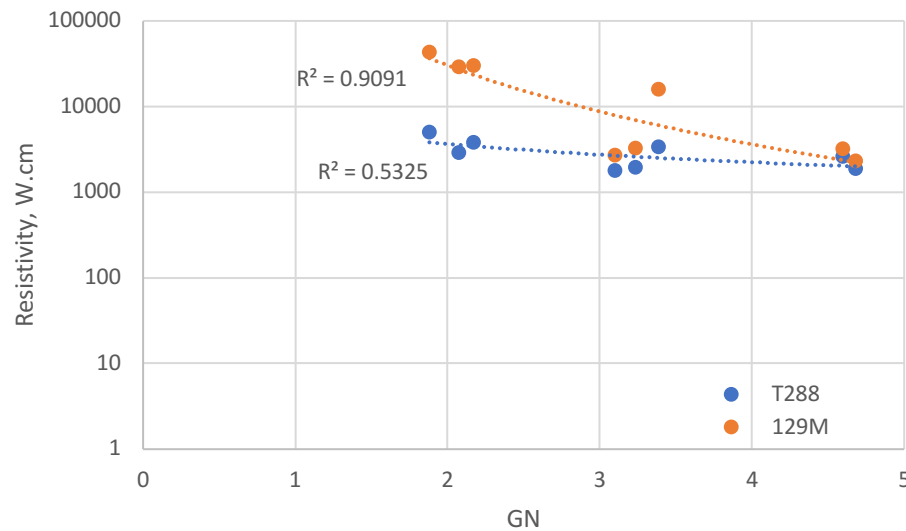Figure 41. Electrical Resistivity as a Function of Grading Number (GN)

Figure 42. Electrical Resistivity as a Function of Fineness Modulus
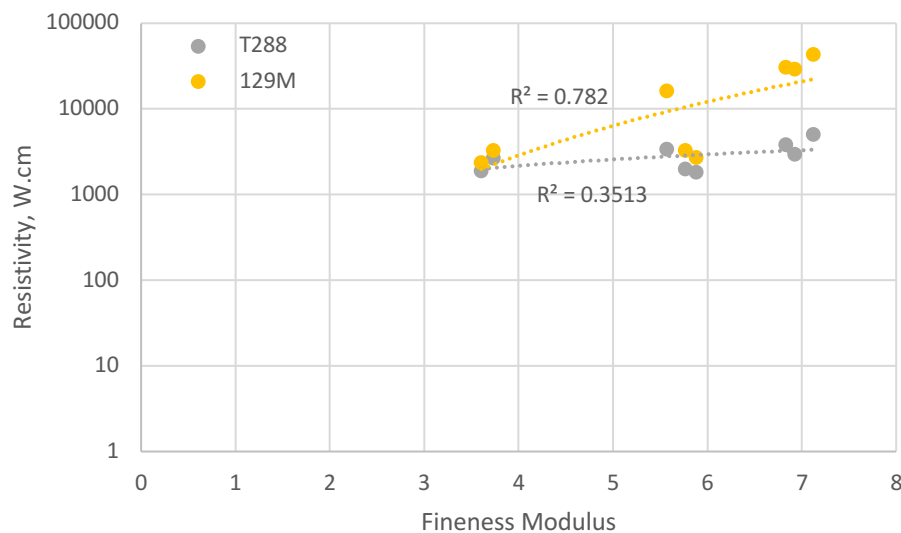
4.3 pH

Figure 43 provides the pH results for selected samples using the AASHTO T 289 standard, which can only be applied to fine samples included in this study because there are not enough materials passing a 2 mm (#10) sieve from coarse samples. Presented values typically indicate the average of three values with minor variations shown. Figure 44 compares these results and values obtained from a third-party laboratory for verification purposes. The third-party laboratory procedures followed California Test 643, which is similar to AASHTO T 289. The difference between these values is about 6.6% or between 0.2 and 0.6 pH, except for one sample, where the difference is 1.3. Based on the 0.31% COV (Coefficient of Variation) of the T 289 results for LWF2, this third-party result appears to be an outlier.

Figure 43. pH of Selected Samples Using AASHTO T 289
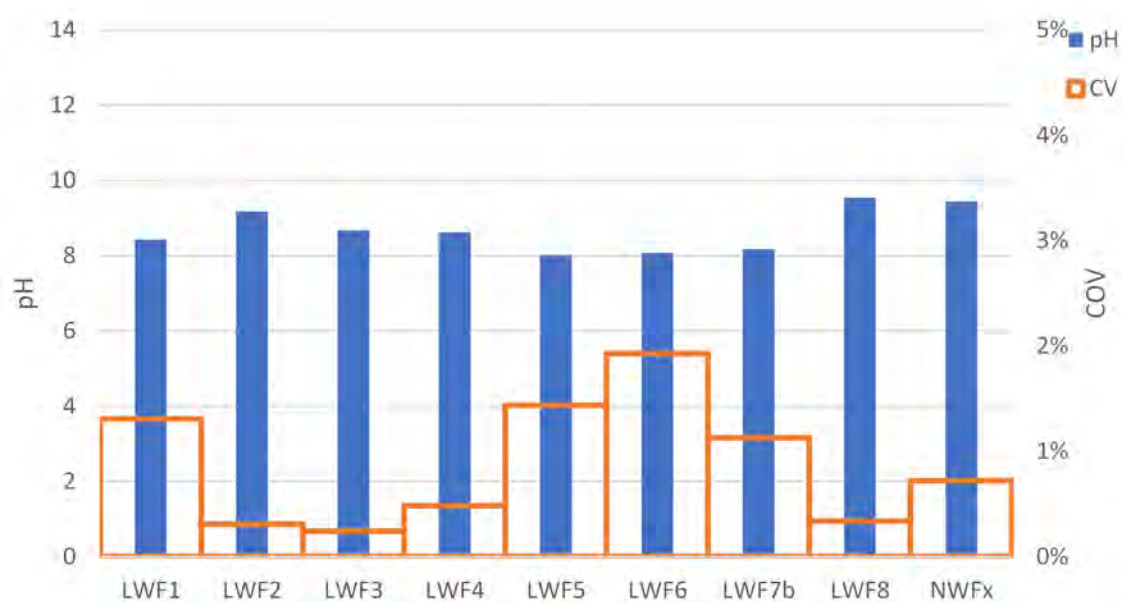
Figure 44. Verification of AASHTO 289 pH Results Using third-Party Laboratory Results
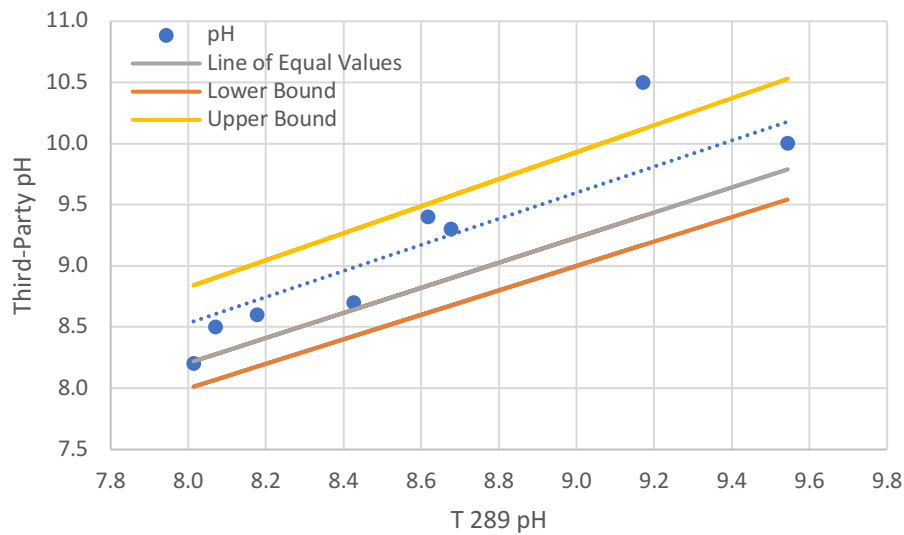
Figure 45 provides an overview of pH results obtained from T 289 and D4972 standards for fine and 21–06, 620-M standards for coarse samples with detailed comparative charts shown in the following figures. The 24-hour saturated condition applies to tests on the aqueous contents obtained from corrosion tests. Figure 46 compares pH values obtained from the fine aggregate samples passing a 2 mm (#10) sieve using AASHTO T 289 and TX-620-M standards. This comparison reveals that the testing method impacts approximately 2.1% of the overall results, but the difference for individual samples varies between 0.2 and 1.4 pH, with the larger difference of 1.4 being chemically significant. Similar observations apply to results from ASTM D4972 with a 2.4% difference in the overall results and sample differences between 0.1 and 0.4 pH, except for one sample having a 0.7 difference, as shown in Figure 47.

Figure 45. Comparison of Recorded pH Values from Different Sources and Test Methods
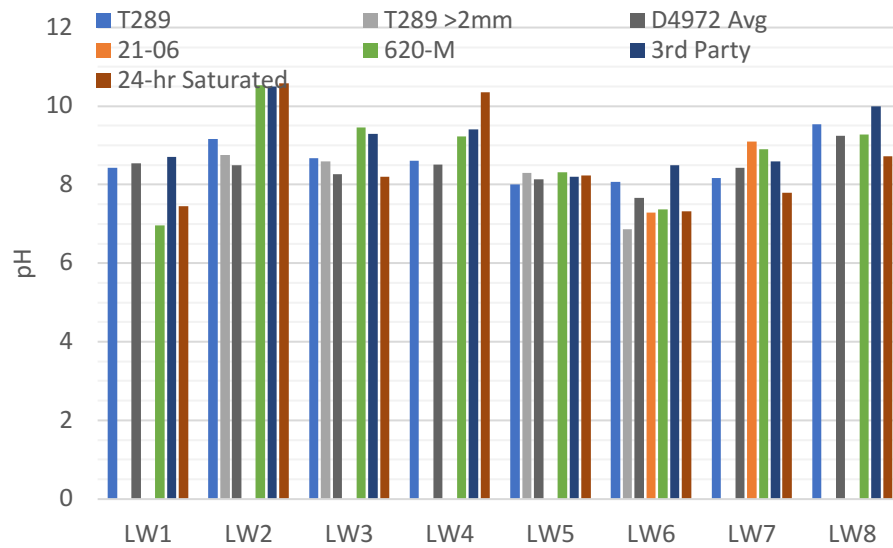
Figure 46. Comparison of pH Results from AASHTO T 289 and TX-620-M Tests
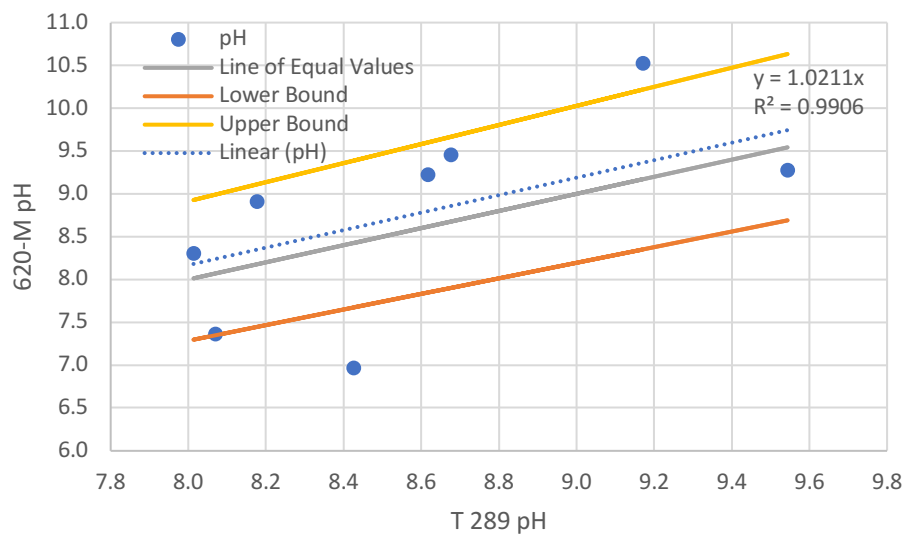
Figure 47. Comparison of pH Results Using AASHTO 289 and ASTM D4972 Tests
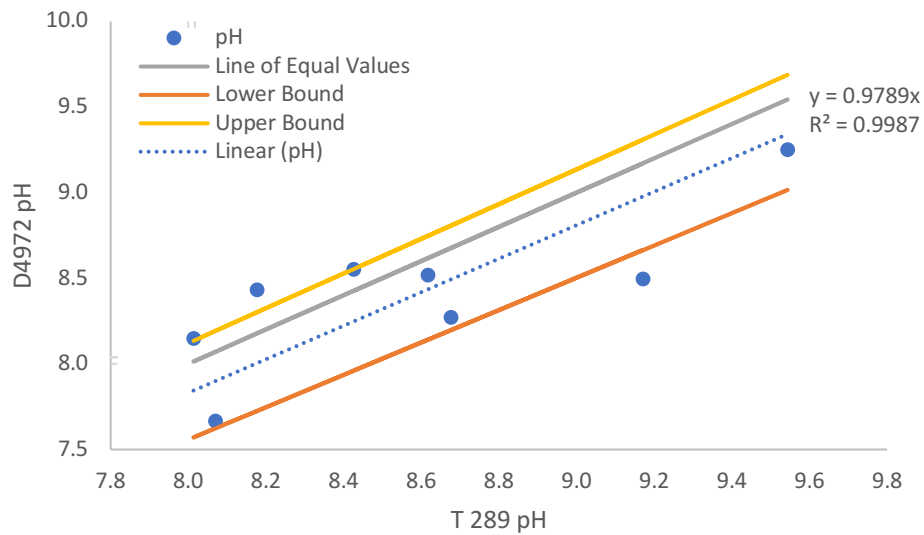
Figure 48 provides a comparison between the results from testing the portion of fine aggregates passing the 4.75 mm (#4) sieve and retained in the #10 sieve to results from testing only the part which passes the 2 mm (#10) sieve, i.e., in accordance with AASHTO T 289. These results demonstrate minor sensitivity to size with a 4.2% difference, except for one sample, where the difference is nearly 15% or 1.2 pH.

Figure 48. Comparison of pH Results Using AASHTO 289 for Materials Passing the 4.75 mm (#4) Sieve but Retained on the 2 mm (#10) Sieve Versus Passing the 2 mm (#10) Sieve

Figure 49 depicts the relationship between electrical resistivity and pH values using AASHTO T 288 versus T 289, and AASHTO T 288 versus ASTM D4972 standards for fine samples passing the 2 mm (#10) sieve, and Texas DOT 129-M versus 620-M standards for coarse and blended samples. The significant variation of resistivity obtained from the 129-M standard is due to the inclusion of various as-is gradations in the test, as opposed to the T 288 standard that is conducted on one specific size only. All three trends suggest a negative correlation between electrical resistivity and pH, but the low fidelity of the correlations rejects a strong influence of pH on the resistivity measurements.
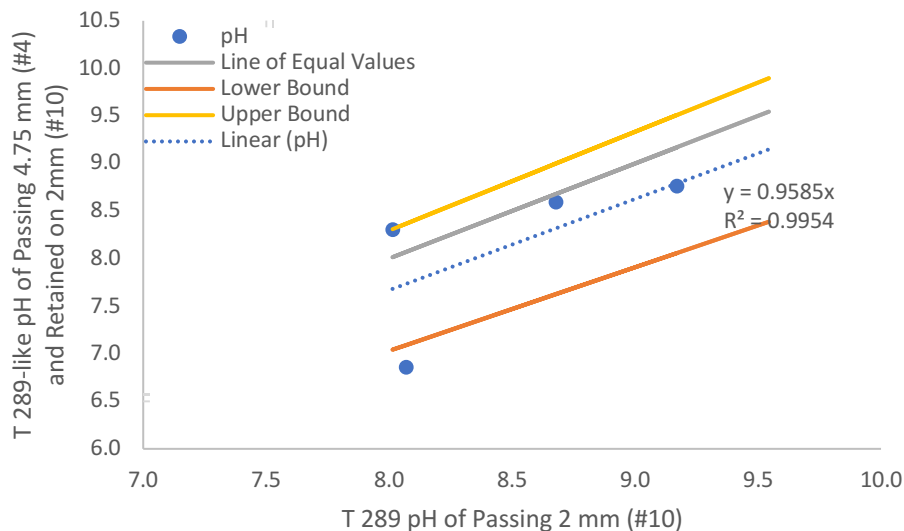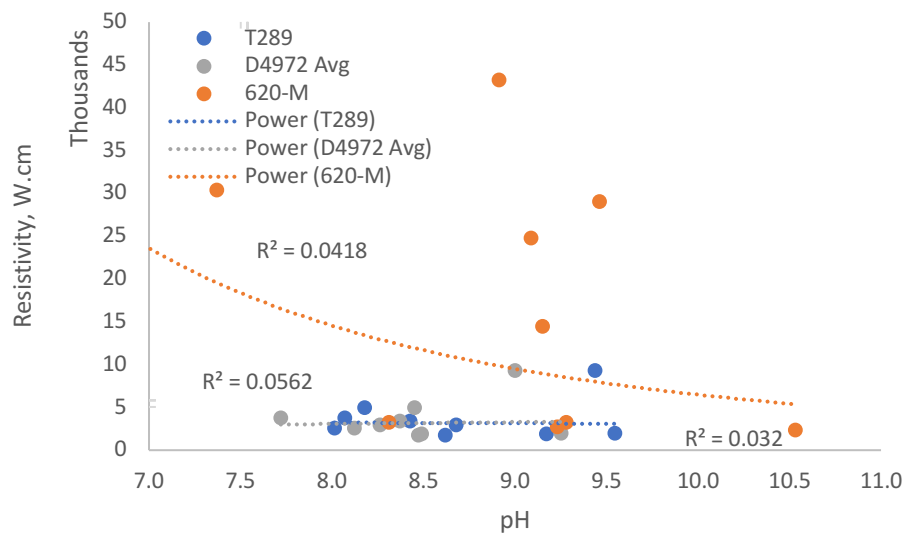
Figure 49 Electrical Resistivity as a Function of pH

This relationship requires further discussions concerning sulfate and chloride contents, as alkaline soils and aggregates might be either salt-affected or calcareous. Calcareous materials contain carbonates such as calcite (calcium carbonate), dolomite (calcium-magnesium carbonate), sodium carbonates, and sulfates. These materials are characterized by alkaline pH, which is less than 8.5. Sodic soils are characterized by a high pH, usually higher than nine, and the major corrosive solutes comprising mineral salts include sodium cations and chloride and sulfate anions. The next section follows with discussions on sulfate and chloride contents.

4.4 Sulfate and Chloride

Figures 50 and 51 show the sulfate and chloride contents obtained from different testing methods. The results represent photoelectric measurements only. Specifications of the testing apparatus and the preliminary observed values showed that the gravimetric methods did not have adequate precision. The AASHTO T 290 and T 291 standards and the third-party verification tests represent samples passing the 2 mm (#10) sieve, and the 620-M standards apply to other samples that were blended or those with coarse gradations. The 24-hour saturated condition relates to corrosion tests on coarse and blended gradations. Sulfate and chloride concentrations are adjusted for the weight of the solid to convert from mg/l to the reported units of mg/kg. The same applies

to aqueous samples extracted from the aggregates in the test box, where the total weight of the aggregate and the total water added, including the water absorbed by the aggregates and surrounding them, were recorded.

Figure 50. Comparison of the Sulfate Contents of Selected Samples Using Different Standards

Figure 51. Comparison of the Chloride Contents of Selected Samples Using Different Standards
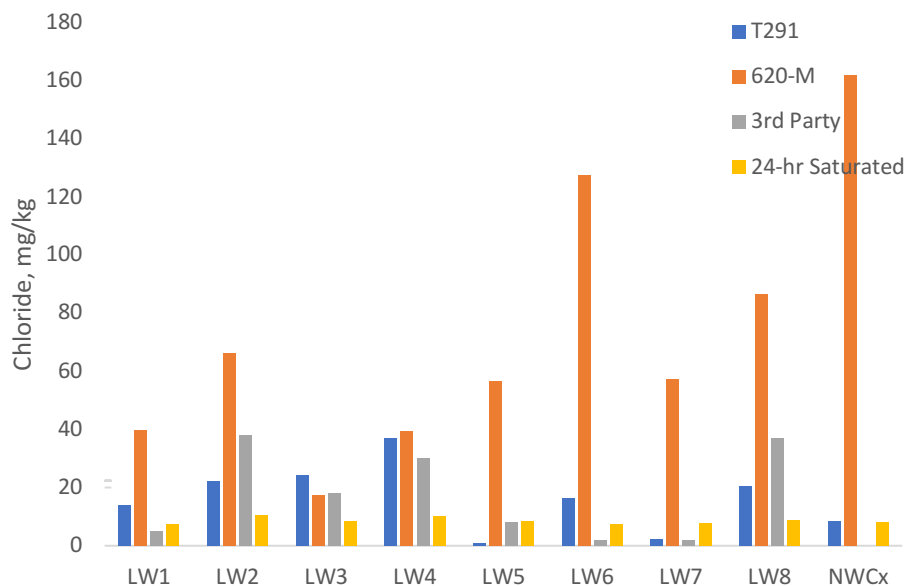
Sulfate contents obtained from AASHTO T 290 and TX-620-M are comparable, however, third-party verification results report nearly 51% larger values, as shown in Figure 52. A close examination of this figure reveals that the gap between results is larger for smaller values of measured sulfate contents and hence could be related to the accuracy of the employed apparatus in this research project compared to the high precision tools used in larger certified laboratories, such as the third-party laboratory.

Figure 52. Verification of Sulfate Results with the Third-Party Laboratory Results
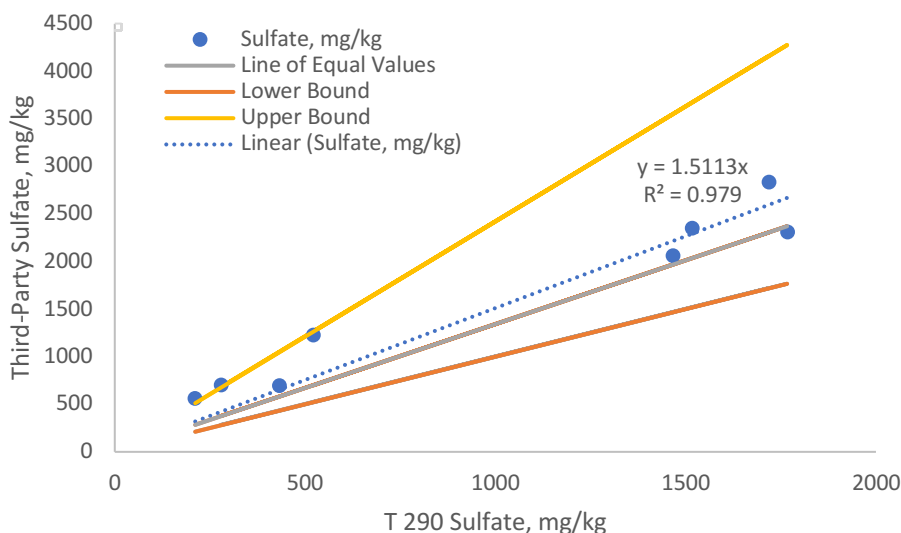
Similar observations for chloride contents show a much better comparison between AASHTO T 291 and the results obtained from third-party verification with an approximate difference of 2.8%, as shown in Figure 53. However, the results from TX-620-M for coarse aggregates are higher (for 8 out of 9 cases) than those measured from fines passing the 2 mm (#10) sieve in accordance with AASHTO T 291. This observation might be due to a longer mixing time in 620-M compared to testing via T 291. The low chloride content might have masked the influence of apparatus choice, which appeared to be a parameter in sulfate measurements.

Figure 53. Verification of Chloride Results with the Third-Party Laboratory Results

Figures 54 and 55 provide more detailed comparisons between AASHTO and TX-DOT methods for measuring sulfate and chloride contents. The T 290 and T 291 results are from testing the portion of the sample passing the 2 mm (#10 sieve), or a similar representative sample from the same source, while the 620-M results are from testing on the full gradation of blended and coarse samples. These figures confirm prior observations and further indicate the higher fidelity of relationships between sulfate measures obtained from referenced standards than chloride measures.

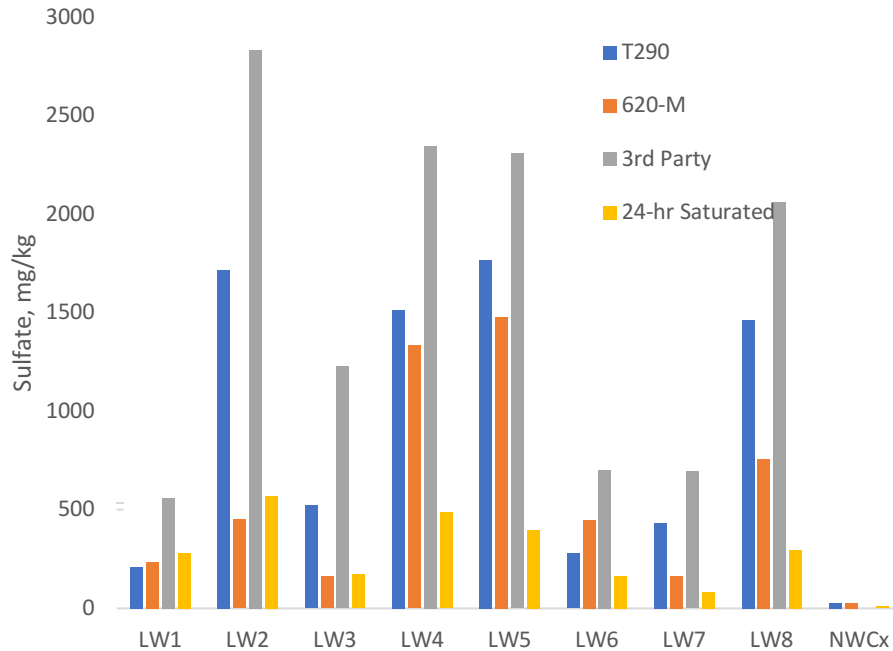Figure 54. Comparison of the Sulfate Contents of Selected Samples Using AASHTO and TX-DOT Standards

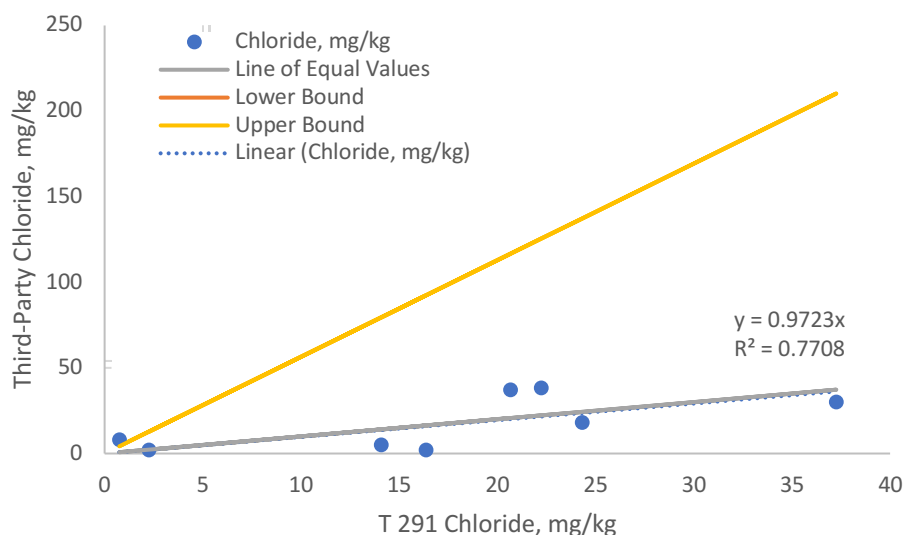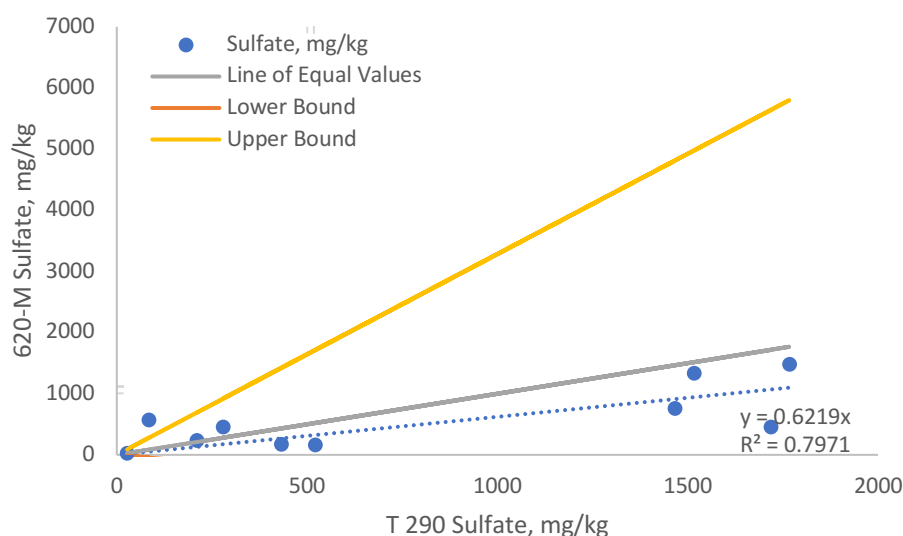Figure 55. Comparison of the Chloride Contents of Selected Samples Using AASHTO and TX-DOT Standards
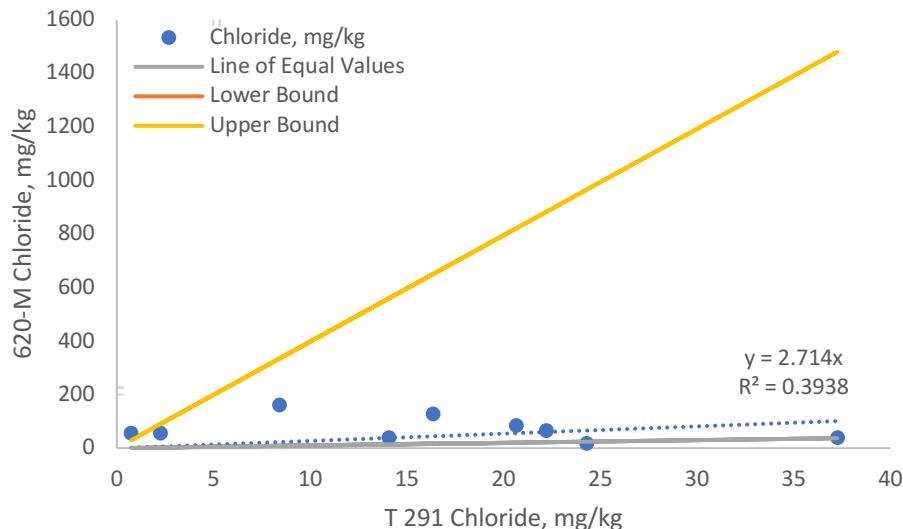
Figures 56 and 57 depict the relationship between electrical resistivity and sulfate-chloride contents. All trends suggest a reduction of electrical resistivity for high values of sulfate and chloride contents. The negative correlations between resistivity and sulfate content have higher coefficients of determination compared to those between resistivity and chloride content, most likely due to higher concentrations of sulfate than chloride contents, which affects the resolution.

Figure 58 exhibits the same relationship for the combined chemical activities of sulfate and chloride contents. Sulfate contents vary between 0.56 and 37 mEq/kg (SO_4^{--} with a valence of 2 mEq/mmole and molecular weight of 96 mg/mmole), and chloride contents vary between 0.021 and 4.6 mEq/kg (Cl^- with a valence of 1 mEq/mmole and molecular weight of 35.5 mg/mmole). Data points for blended and coarse-graded samples with significant fine contents are close to the trendline of results from tests conducted on samples that only include portions passing the 2 mm (#10) sieve. Those with negligible fines show substantially higher resistivity. This difference explains the lower coefficient of determination of the trendline representing blended and coarse samples as opposed to the result from testing samples that only include portions passing the 2 mm (#10 sieve).

Figure 56. Electrical Resistivity as a Function of Sulfate Contents
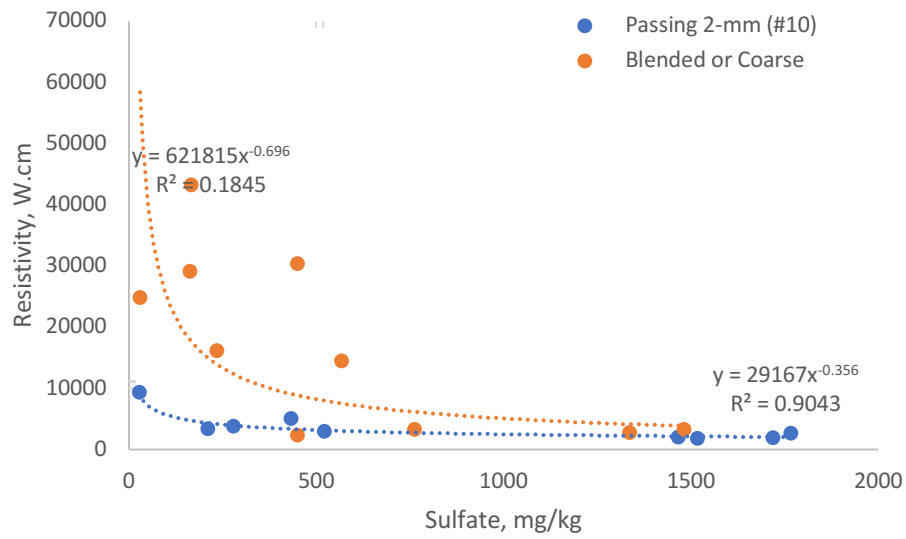
Figure 57. Electrical Resistivity as a Function of Chloride Contents
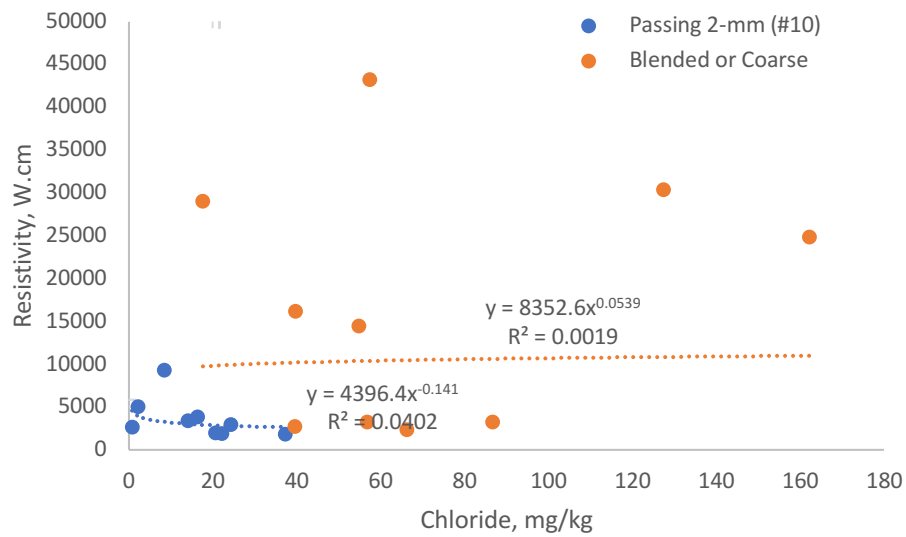
Figure 58. Electrical Resistivity as a Function of Combined Sulfate and Chloride Milliequivalent Units
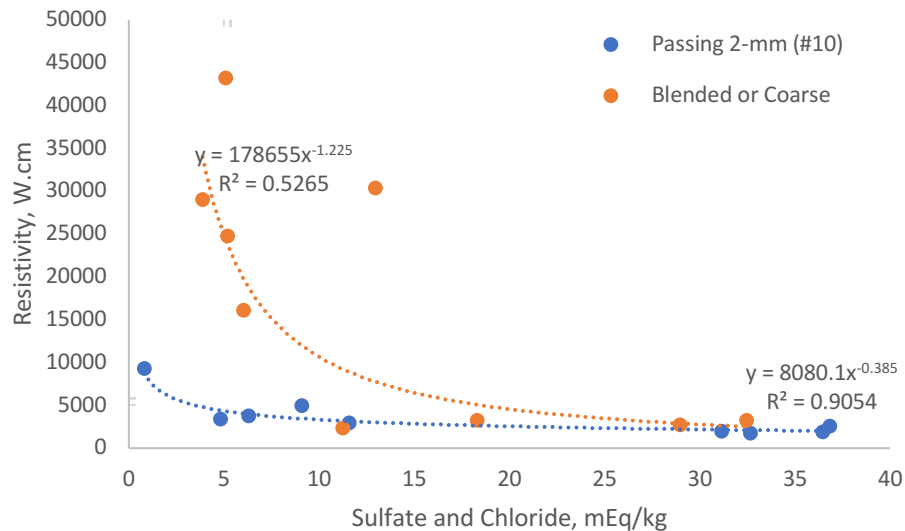
Following prior discussions with respect to pH, Figures 59 and 60 show the trends of pH values versus sulfate and chloride contents for AASHTO and TxDOT standards, representing fine and blended samples, respectively. Trendlines show no effect of ions on pH, except for chloride ions corresponding to tests on portions passing the 2 mm (#10 sieve), but with a low coefficient of determination. The lack of correlation might be related to other ions, such as calcium, that affect the pH but are not measured directly in this study.

Figure 59. pH as a Function of Sulfate Contents
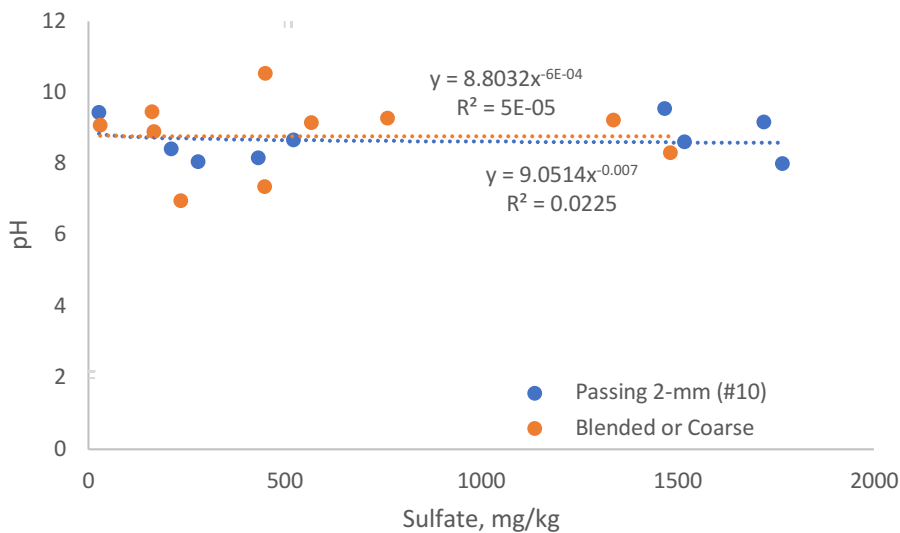
Figure 60. pH as a Function of Chloride Contents

The chart shows pH on the y-axis (0 to 12) and Chloride, mg/kg on the x-axis (0 to 180), with two data series:
- Passing 2-mm (#10): $y = 8.1524x^{0.0261}$, $R^2 = 0.2355$
- Blended or Coarse: $y = 9.5943x^{-0.022}$, $R^2 = 0.0138$
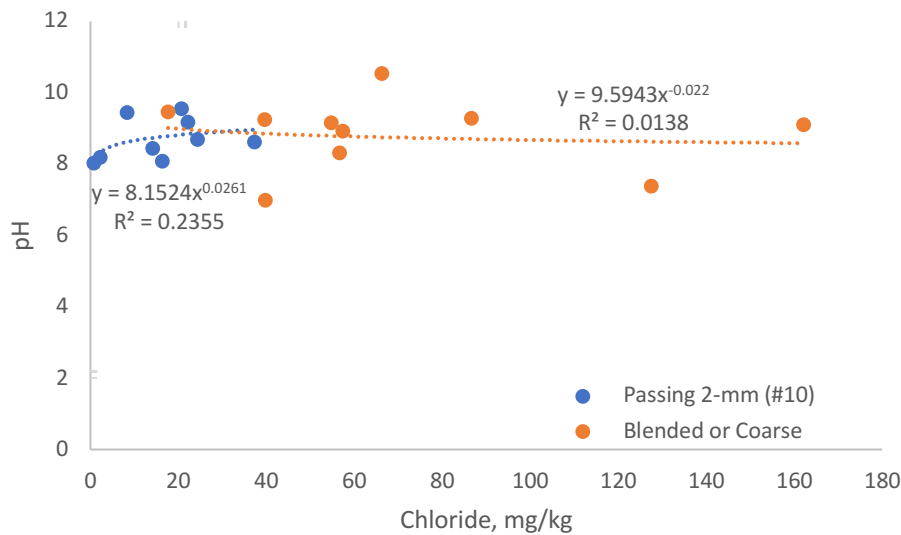
4.5 Corrosion Rate

Corrosion rate testing included blended samples containing coarse aggregates, LW1 to LW8. Two samples, LW2 and LW5, contained more than 80% fines, passing the 4.75 mm (#4) sieve. Three samples, LW1, LW4, and LW8, had between 20% and 35% fines, and other samples, LW3, LW6, and LW7, had less than 1% fines, as shown in Figure 27. The NW sample had nearly 10% fine content. Figure 61 compares the corrosion rate of galvanized steel coupons immediately after insertion into the submerged aggregate samples. Figures 62 and 63 show the changes in corrosion rate during the following cycles, as shown in Table 8:

- Wetting: ASTM Type II deionized water was added to pre-compacted aggregate samples to fill the plastic container. The sample was then tested for corrosion rate and electrical resistivity.
- Saturation: Wetted aggregates were maintained in the closed plastic box for 24 hours. The sample was then tested for corrosion rate, electrical resistivity, sulfate and chloride contents, and pH.
- Drainage: The sample was drained at free atmospheric pressure and tested for corrosion rate and electrical resistivity.
- Air drying: Moist aggregates were maintained in the closed plastic box for consecutively increasing periods, so rewetting happens on days 7, 14, 28, 91, 182, and 364. Samples were then tested for corrosion rate and electrical resistivity before rewetting and resuming the cycle. This report covers Cycles 1, 2, and 3 for the first 28 days of observation. Future amendments will cover complete cycles for a year.

Table 8. Summary of Moisture Cycles During Corrosion Tests

Day	Wetting	Saturation	Drainage	Air Drying
Cycle 1	0	0–1	1	1–7
Cycle 2	7	7–8	8	8–14
Cycle 3	14	14–15	15	15–28
Cycle 4	28	28–29	29	29–91
Cycle 5	91	91–92	92	92–182
Cycle 6	182	182–183	183	183–364

The corrosion rate for the wet cycle in Figure 61 is the average of measured values upon adding water and just before draining over 24 hours in Cycle 1. The corrosion rate for the moist cycle in the same figure is the average of measured values after drainage and before rewetting over the specified period in each cycle for air drying, e.g., seven days for Cycle 1. These results indicate that all coarse lightweight aggregate samples have lower corrosion rates than coarse normal-weight aggregate samples. Further, the average corrosion rate of moist samples is considerably lower than those of wet samples. The difference is larger for coarse blends compared to fine samples, as fine samples retain more moisture after drainage and during air drying.

The saturation process does not significantly affect the corrosion rate, but draining the sample reduces the corrosion rate by one to two orders of magnitude. Further, corrosion rates after the rewetting are typically smaller than the original values. The initial corrosion rate for carbon steel coupons is nearly 25% more than for galvanized steel coupons (Figure 64). Figure 65 compares the same rate for the total estimated corrosion over the observed period, indicating a 35% higher carbon rate than galvanized steel.

Figure 61. Initial Corrosion Rate of Galvanized Steel Coupons
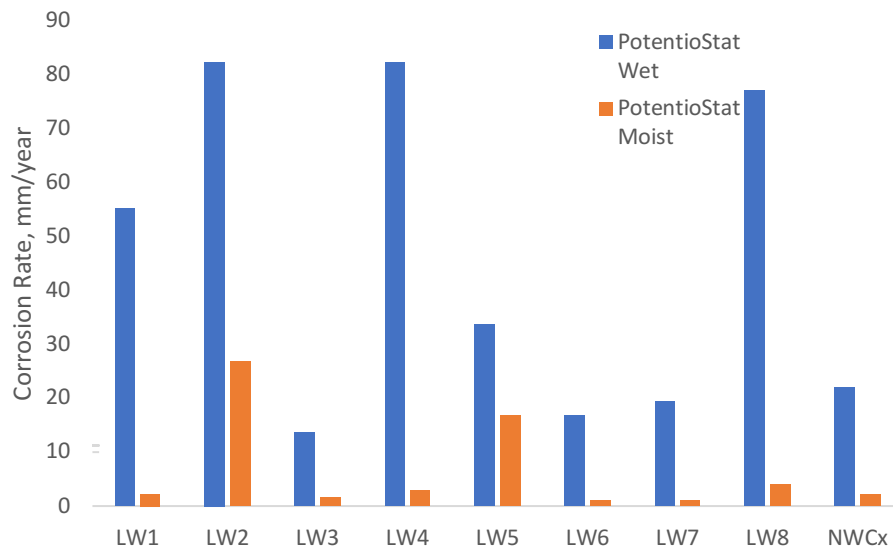
Figure 62. Corrosion Rate of Galvanized Steel Coupons During Wetting and Drying Cycles
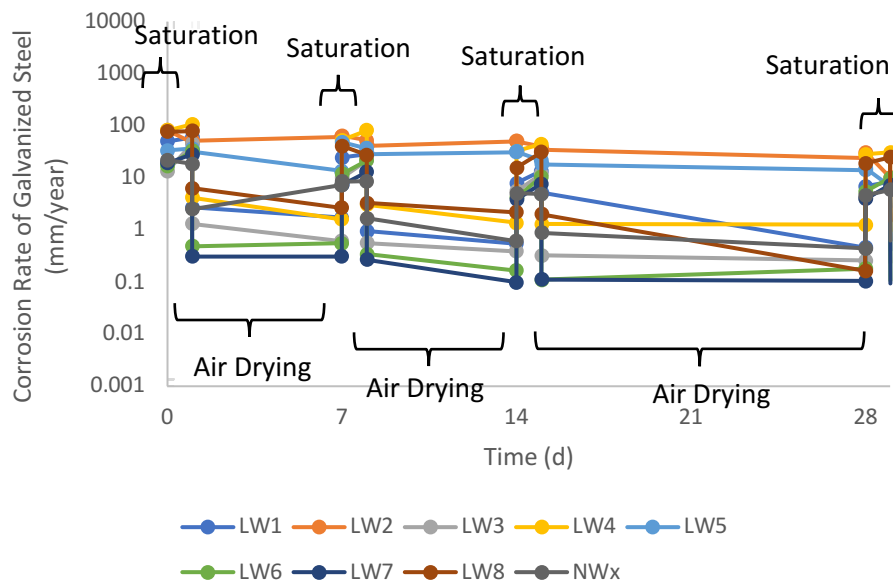
Figure 63. Corrosion Rate of Carbon Steel Coupons During Wetting and Drying Cycles
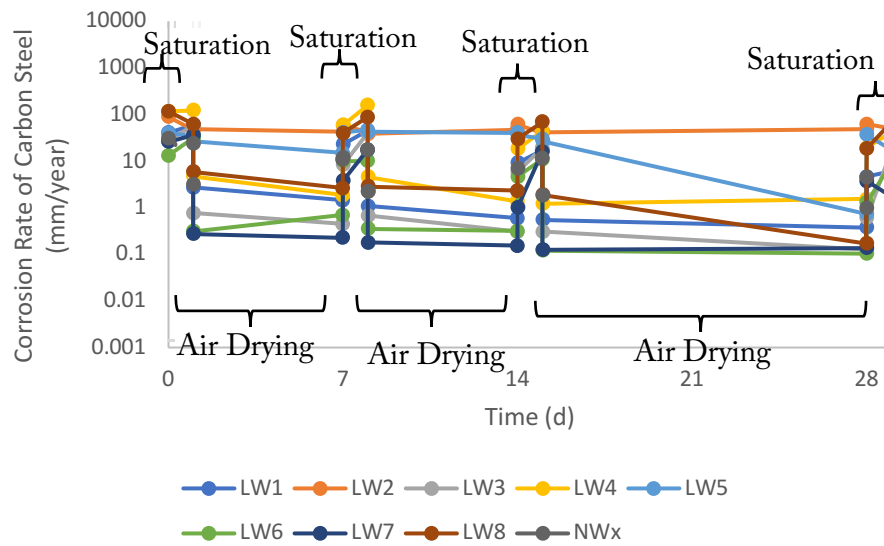
Figure 64. Comparing Corrosion Rates of Galvanized and Carbon Steel Coupons
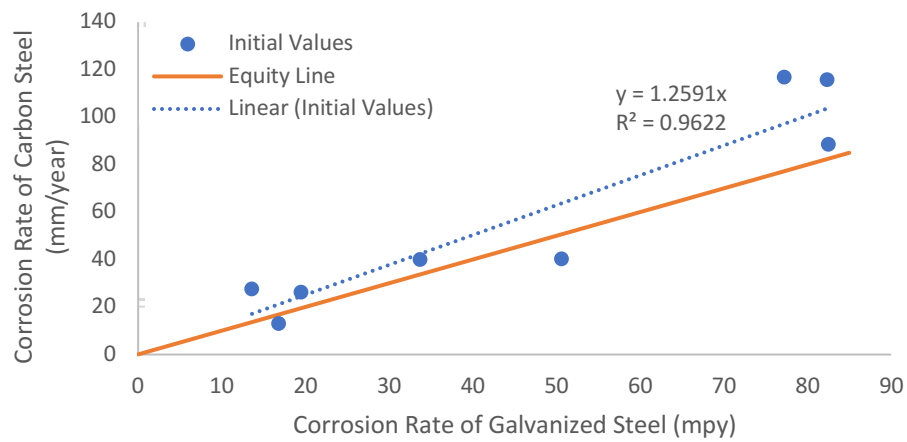
Figure 65. Comparing Total Corrosion Rates of Galvanized and Carbon Steel Coupons over 28 Days
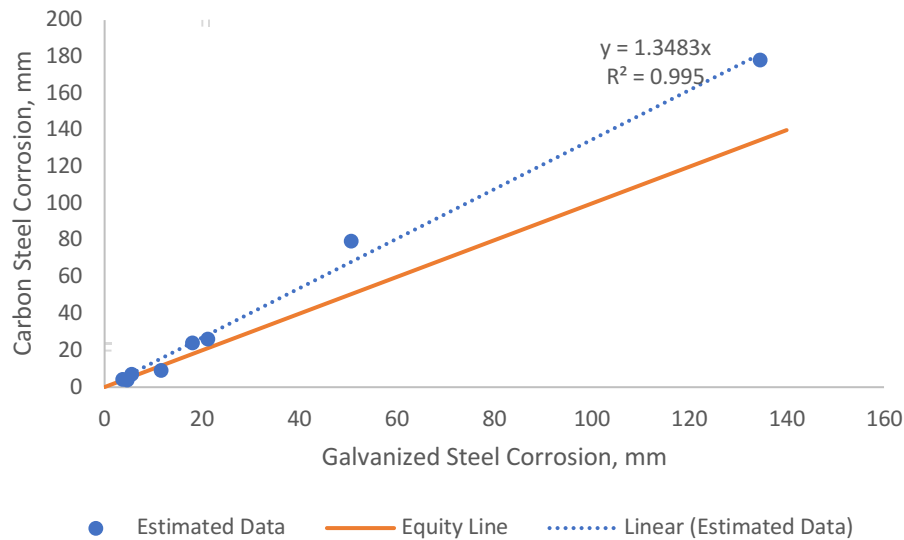
Figures 66 and 67 exhibit patterns of changes in electrical resistivity during wetting, saturating, drainage, and air-drying cycles. The electrical resistivity followed the two-electrode measurement technique using a soil box with a volume of 2,839 ml (3 quarts). Aggregates were placed and compacted in plastic containers following the standard practices described in TxDOT 129-M. The drainage involved the extraction of aqueous contents through a 4.3 mm (0.17") diameter plastic tube. The electrical resistivity of the aqueous contents was measured using the 75- and 280-ml volume soil boxes. Measured values indicate that the normal weight aggregate had the highest resistivity for aqueous contents, although these aggregates did not show the lowest corrosion rate or the highest resistivity of aggregate samples.

Figure 66. Electrical Resistivities During Wetting and Drying Cycles
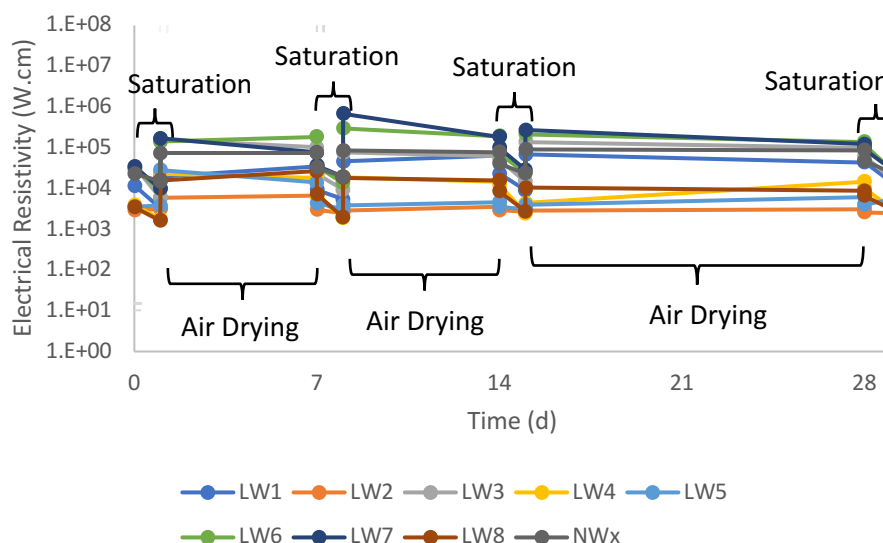
Figure 67. Aqueous Electrical Resistivities During Wetting and Drying Cycles
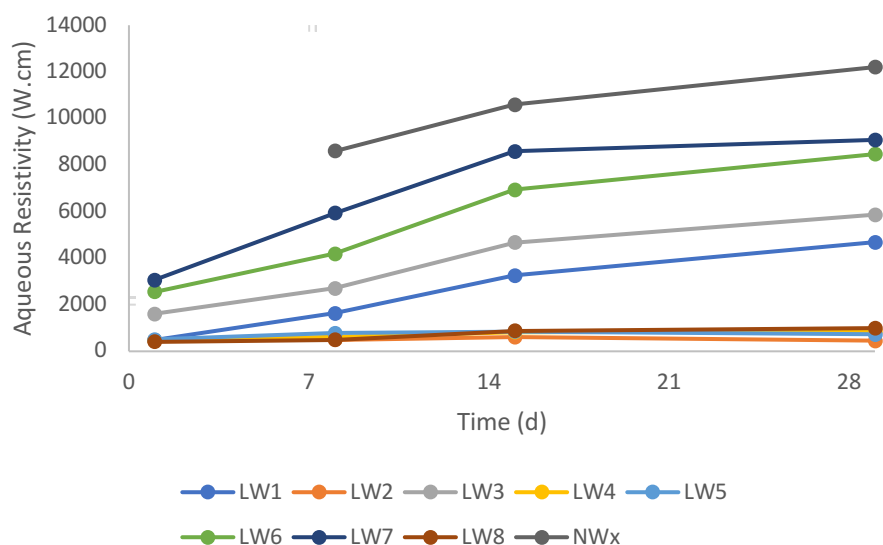
The pH was also measured immediately for the aqueous contents, as shown in Figure 68. Sulfate and chloride contents were measured for the filtered aqueous contents passing the 0.45 micrometer (Grade 42) qualitative filter paper (Figures 69 and 70). Changes in these properties are typically commensurate with observed trends of corrosion rates, where each cycle results in higher resistivity, lower sulfate and chloride contents, and lower corrosion rates, with some exceptions. However, cycles of wetting and drying do not appear to have a substantial influence on pH values. Notably, the normal-weight sample has lower sulfate and chloride contents than most lightweight aggregates, consistent with observations of higher electrical resistivity. Hence, it is essential to note that coarse lightweight aggregate samples show lower corrosion rates despite lower resistivity and higher ion contents.

Figure 68. pH Values During Wetting and Drying Cycles
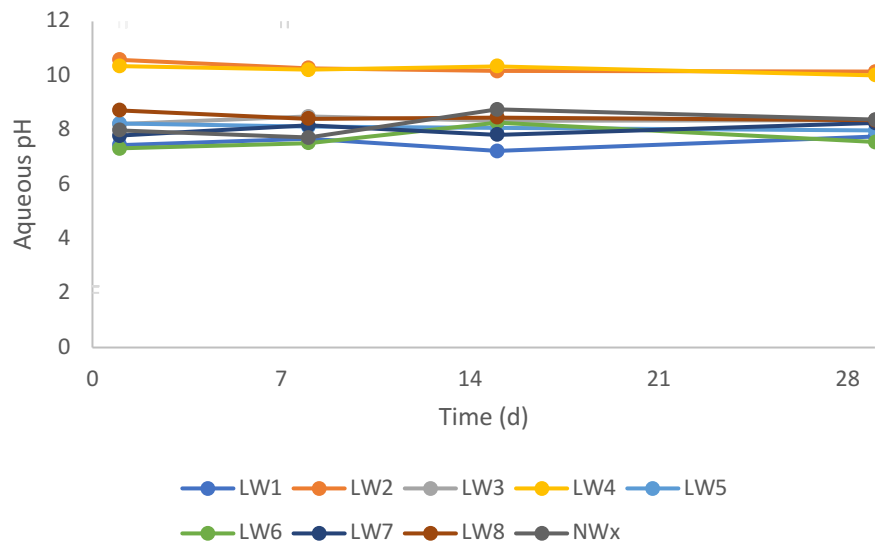
Figure 69. Sulfate Contents During Wetting and Drying Cycles
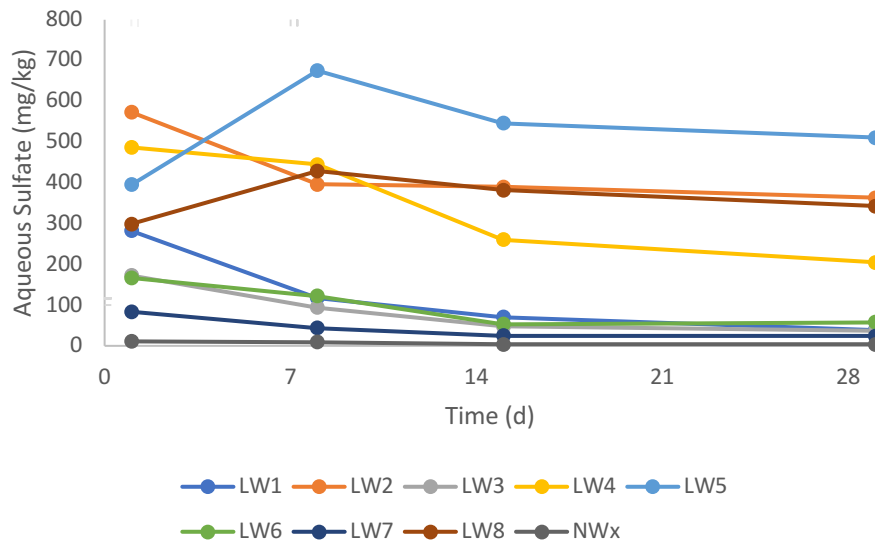
Figure 70. Chloride Contents During Wetting and Drying Cycles
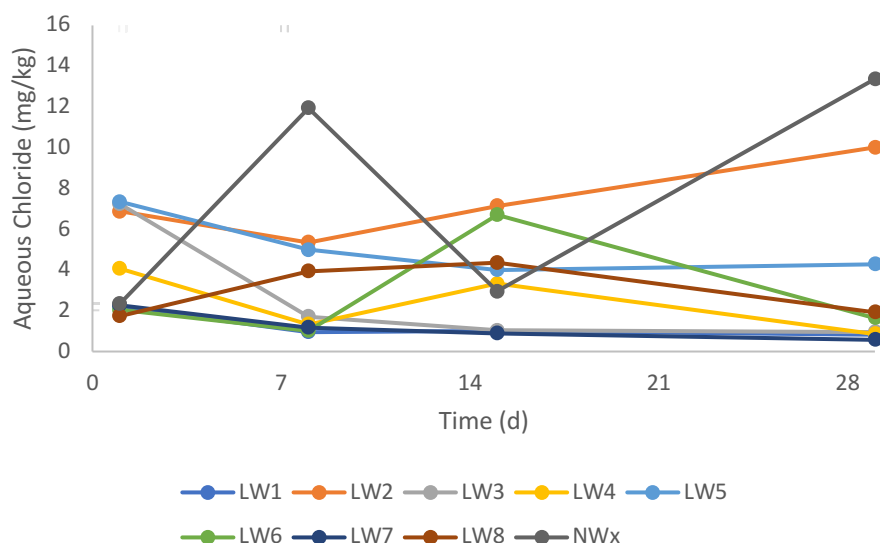
Figure 71 presents the relationship between corrosion rate and electrical resistivity. Fitted power functions indicate the drop of corrosion rates as the electrical resistivity of selected aggregates rises (i.e., negative correlation between corrosion rate and resistivity). As shown in prior observations, the corrosion rate of galvanized steel is lower than that of carbon steel. Trends depicting correlations between electrical resistivity and corrosion rates that consider electrical resistivity measured from wet or moist aggregate in the corrosion testing box compared to the correlations with resistivity/conductivity measured from the aqueous content obtained after draining the aggregates are similar. The rate of decline depicted by the trends is highest for moist aggregates, i.e., the average values from drained and air-dried conditions, and is 0.877 and 0.921 for carbon and galvanized steel, respectively. Trends for wet aggregates, during the average 24-hour saturation period, have the lowest rate of decline, equal to 0.652 and 0.622 for carbon and galvanized steel, respectively. Coefficients of determinations of trendlines vary between 0.645 and 0.835, indicating approximately similar fidelity for various fitting curves.

Figure 71. Variation of Corrosion Rates as a Function of Electrical Resistivity
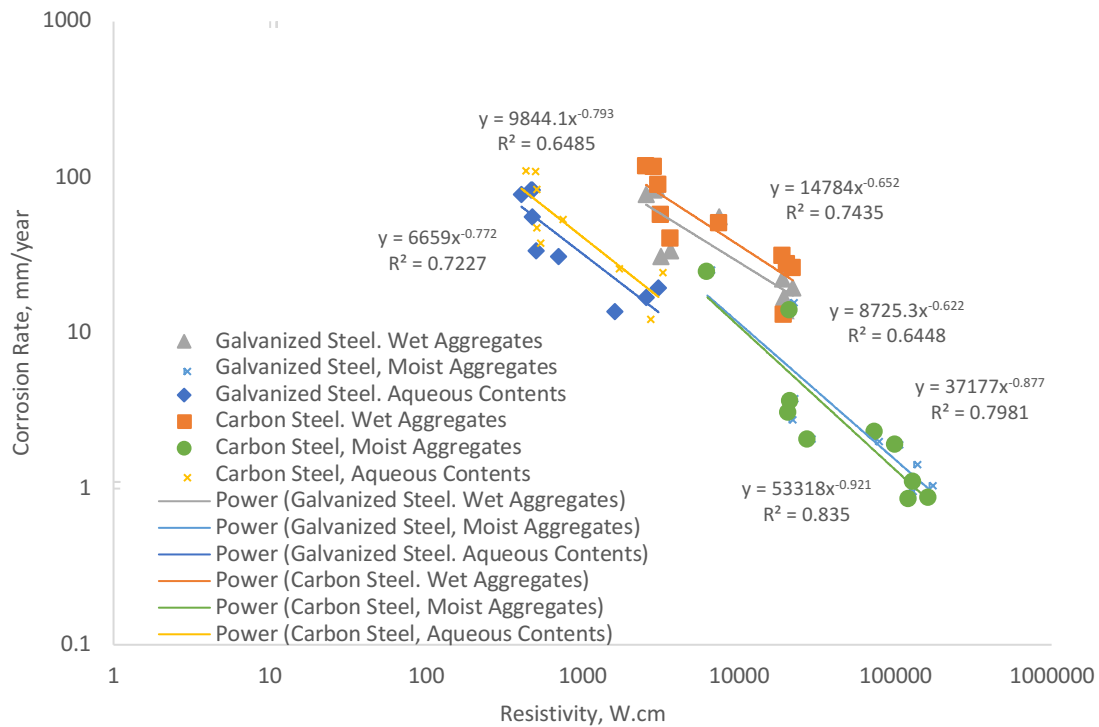
The analysis of test results indicates a weak correlation between corrosion rates and pH values of wet aggregates, as shown in Figure 72. Regardless, these curves confirm the higher corrosivity of carbon compared to galvanized steel and suggest a higher rate of increase for carbon steel as a function of pH.

Figure 72. Variation of Corrosion Rates as a Function of pH
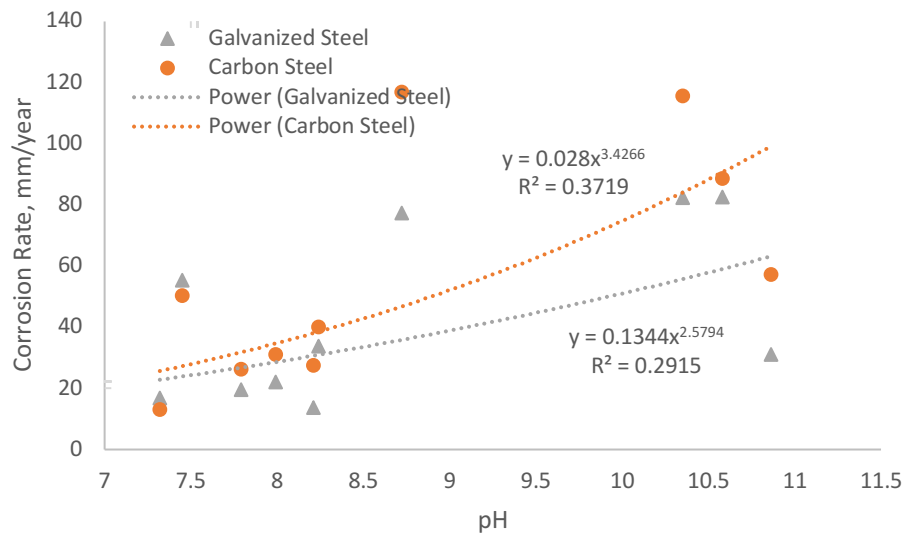
Figures 73 and 74 depict the variation of corrosion rates of wet aggregates as a function of sulfate and chloride contents. Sulfate and chloride contents represent the tests performed on the aqueous contents drained from the corrosivity soil boxes. These values may differ from sulfate and chloride contents obtained from soil box tests using AASHTO and TxDOT standardized procedures, but the overall trend of increasing resistivity shown in Figures 56 and 57 align with the reduction of corrosion rates in Figures 73 and 74. Trends indicate a weak correlation between sulfate content and corrosion rate, and a negligible one with respect to chloride contents. Regardless, with few exceptions, materials with high sulfate contents are typically associated with relatively high corrosion rates. The same applies to chloride measures. Figure 75 exhibits these trends for the total contents of sulfate and chloride in mEq/kg. These trends are closer to those for sulfate trends due to relatively higher sulfate contents in the total milliequivalent than chloride contents.

Figure 73. Variation of Corrosion Rates as a Function of Sulfate Content
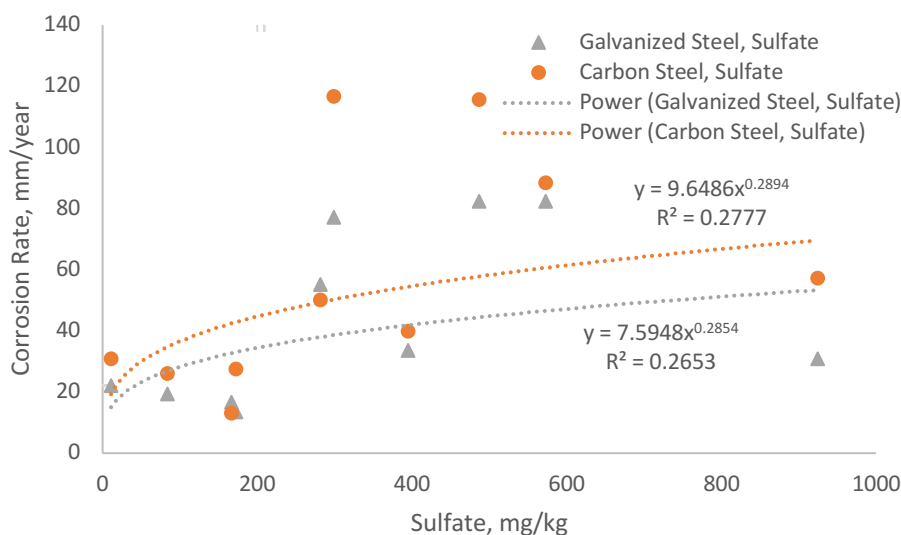
Figure 74. Variation of Corrosion Rates as a Function of Chloride Content
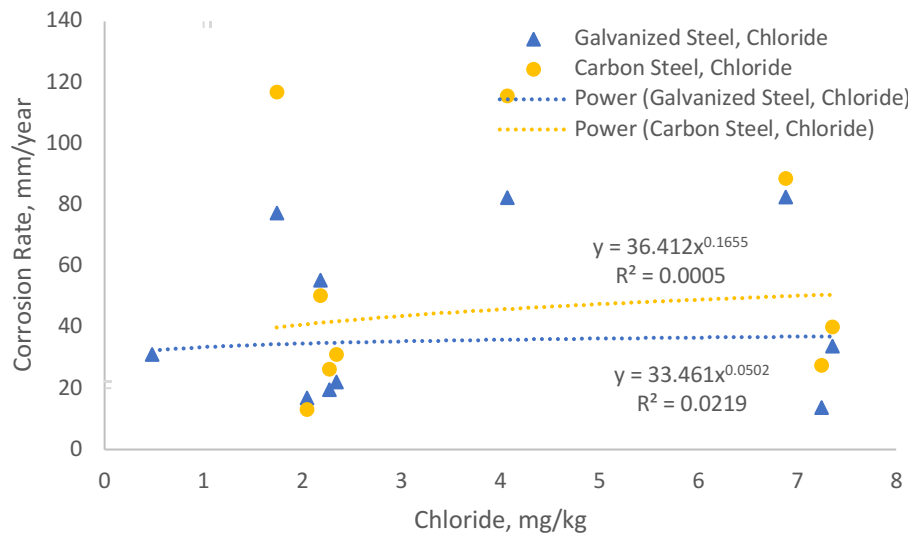
Figure 75. Variation of Corrosion Rates as a Function of Sulfate and Chloride Contents
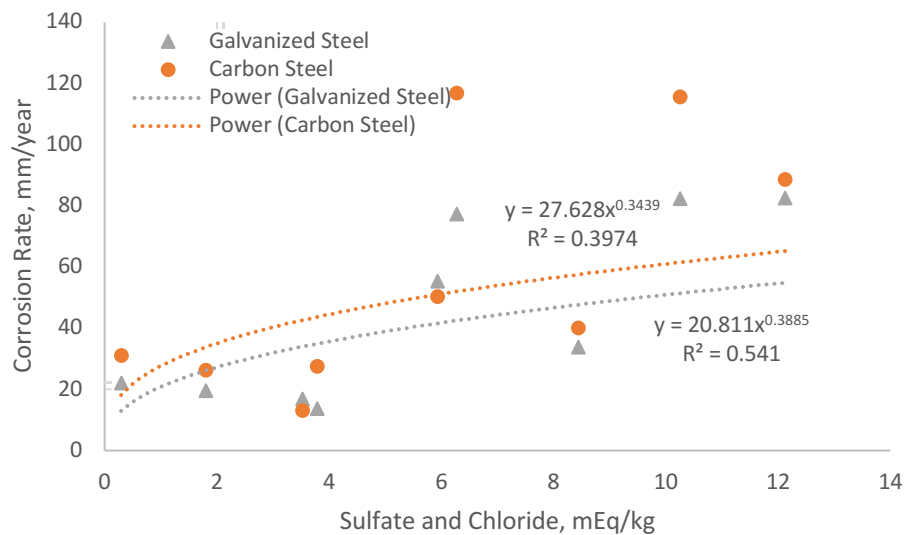
4.6 Thickness Loss

The initial thickness of the zinc coat on galvanized steel coupons was measured to be 20 micrometers on average. A negligible 1-micrometer thick layer was also measured over the carbon steel coupons. Figure 76 displays the corrosion of steel coupons after three months of exposure to wet and dry conditions, listed in Table 8. These images compare normal-weight and lightweight aggregates with similar electrochemical properties.

Figure 76. Examples of Galvanized (Left) and Carbon (Right) Steel Coupons Corrosion Embedded in Normal Weight (Top) and Lightweight (Bottom) Aggregates

Figure 77 shows the measured coating for galvanized and carbon steel coupons. The total thickness of the coat on galvanized coupons is 50% to 87% more than the initial thickness of zinc, indicating the formation of zinc-oxide, which has less density than zinc and increases the coating thickness. This difference is the basis of the calculation of zinc loss. Similarly, the rust thickness over carbon steel, if not already delaminated, may indicate loss of the original steel. The measured thickness of rust varies between 28 and 70 micrometers with two potential outliers of 151 and 4 micrometers suggesting pre- and post-delamination scenarios confirmed by visual inspection. A better assessment of material loss for these cases would be a weight-based analysis to be performed in the long term.

Figure 77. Measured Thickness of the Coating
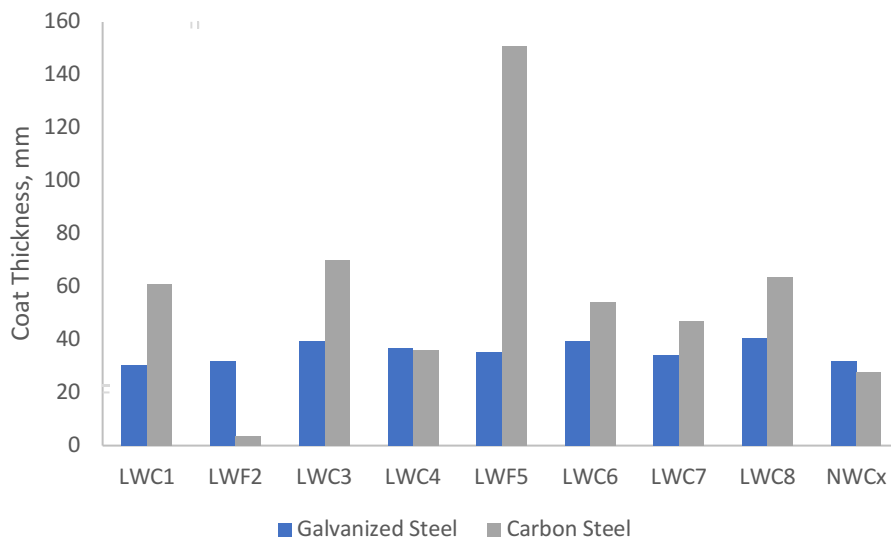
The relationship between thickness loss measures and expected corrosion from electrochemical properties indicates that the corrosion loss is nearly 120% and 250% more than the estimated values for galvanized and carbon steel coupons, respectively (Figure 78). These values require additional verification by weight loss measures in the long term. Figure 79 confirms that the thickness loss of carbon steel is nearly 3.3 times more than galvanized steel based on thickness loss measures.

Figure 78. Relationship Between Measured Thickness Loss and Average Corrosion Rate
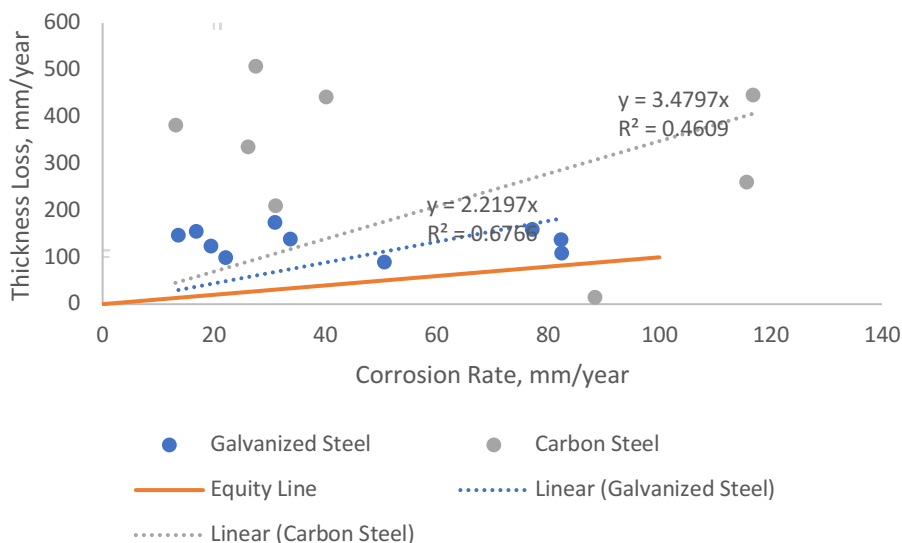
Figure 79. Thickness Loss for Galvanized and Carbon Steel Coupons
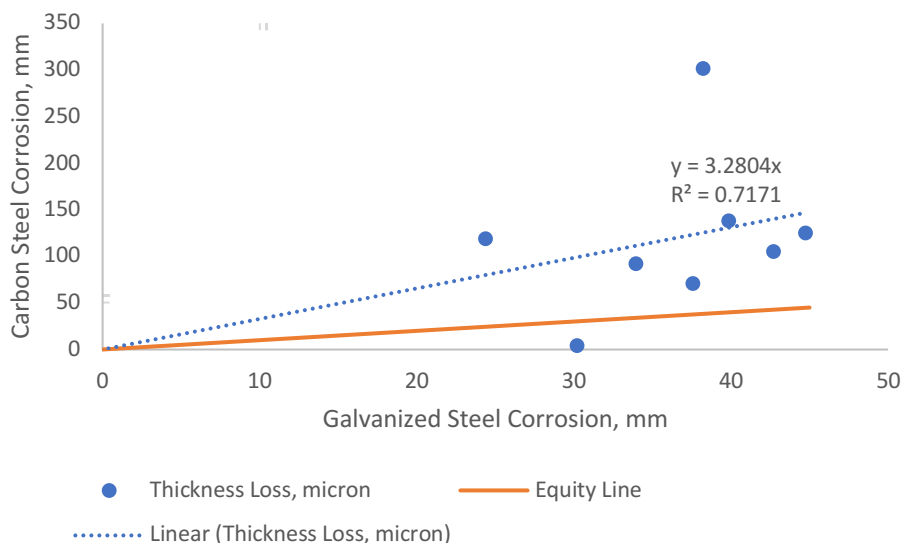
4.7 Performance Analysis

Table 9 provides a summary of lightweight aggregate properties to evaluate a classification of corrosion performance using the results from this research. This table follows NASEM (2021) discussions to classify various parameters and obtain a corrosivity rank. Metal losses are from integrating corrosion rates over 29 days with the consideration of saturated and air-dried conditions. This period includes three wetting cycles, three days of the saturated state, and 26 days of air drying. The corrosion rate for the saturated condition is the average of the measured rate upon wetting and before draining. The corrosion rate for the air-drying period is the average of the measured rate upon draining and before rewetting.

Samples include two fine- (LW2 and LW5) and six coarse-blended (LW1, LW3, LW4, LW6, LW7, and LW8) gradations based on measured percentages passing the 4.75 mm (#4) sieve. Fine samples also have a high content of percentages passing the 2 mm (#10 sieve), which is above 25%. Hence, the electrochemical properties of these samples represent results obtained from AASHTO standards for samples that have been separated on the 2 mm (#10) sieve. For other samples, results are from testing in accordance with the TX-DOT standards for as-is gradations.

The fineness modulus and GN values provide a quantitative representation of the gradation. These values highlight the high percentages of fine contents in three formally classified coarse samples, that is, LW1, LW4, and LW8. Hence, three distinguished groups of aggregates include coarse aggregates with a GN below 3 and FM above 6 (Group 1), coarse aggregates with a GN between 3 and 4 and an FM between 5 and 6 (Group 2), and fine aggregates with a GN above 4 and FM below 4 (Group 3). These groups exhibit different corrosion rates, so the GN may act as a ranking parameter for corrosion classification.

The corrosivity rank represents the influence of resistivity, pH, and sulfate and chloride ion contents on the corrosion rate. The resistivity of Group 1 aggregates is well above 25,000 Ω.cm, indicating minimum corrosion rates and confirming measured values. Group 2 aggregates cover the range of 2,500 to 25,000 Ω.cm. The resistivity of Group 3 aggregates falls within the range of 1,000 to 3,000 Ω.cm. These revised limits differ from those shown in NASEM (2021) for normal weight aggregates.

The thresholds of sulfate and chloride contents to influence corrosion are 200 and 100 mg/kg, respectively. However, the low corrosivity of sample LW6 does not support these triggering values for ESCS. So, raising these thresholds to 500 mg/kg for sulfate and 150 mg/kg for chlorides is considered appropriate. The presented ranking neglects pH values above 6, and hence the pH of lightweight aggregates does not impact their classification. Table 10 summarizes observed ranges for various groups using the suggested ranking parameters in Table 11.

Table 9. Corrosion Rate and Associated Tests

Sample	Gradation	PP 4.75 mm (#4)	PP 2 mm (#10)	FM	GN	Water Absorption, %	Resistivity[1], Ω.cm	pH[1]	Sulfate[1], mg/kg	Chloride[1], mg/kg	Corrosivity Rank	Galvanized Steel Expected 29-day Corrosion, μm	Carbon Steel Expected 29-day Corrosion, μm
LW1	Coarse	31.3	5.35	5.56	3.4	12.3	16,133	7.0	235	39.8	-1	11.6	9.1
LW2	Fine	84.9	58.1	3.60	4.7	7.8	1888	9.2	1719	22.2	-6	134 [2]	178
LW3	Coarse	0.7	0.56	6.92	2.1	12.6	29,050	9.5	162	17.6	0	5.49	7.27
LW4	Coarse	20.2	3.29	5.87	3.1	16.2	2715	9.2	1336	39.6	-5	21.2	26.4
LW5	Fine	87.4	54.5	3.73	4.6	25.0	2630	8.0	1766	0.75	-5	50.6 [2]	79.7
LW6	Coarse	1.0	0.19	6.83	2.2	11.5	30,385	7.4	449	127	-2	4.6	3.8
LW7	Coarse	0.2	0.16	7.12	1.9	3.0	43,244	8.9	167	57.4	0	3.6	4.2
LW8	Coarse	21.8	0.47	5.76	3.2	15.4	3264	9.3	762	86.6	-4	18.0	24.2
NW	Coarse	10.4	3.30	5.97	3.0	0.48	24,812	9.1	29.9	162	-1	7.2	12.1

[1] AASHTO or TX-DOT standards for samples containing more or less than 25% passing the 2 mm (#10) sieve, respectively.

[2] These expected values exceed the initial thickness of the zinc coating and cannot be verified using available galvanized coupons.

Table 10. Range of Corrosion Rates for Aggregate Groups

Group	Samples	GN	Resistivity,[1] Ω.cm	Sulfate,[1] mg/kg	Chloride,[1] mg/kg	Revised Corrosivity Rank	Galvanized Steel 29-day Corrosion, μm	Carbon Steel 29-day Corrosion, μm
1	LW3, LW6, LW7	< 3	> 25,000	< 500	< 150	0	< 5.5	< 7.5
2	LW1, LW4, LW8	3–4	2,500–25,000	500–1,500	< 150	-3	< 25.0	< 30.0
3	LW2, LW5	> 4	1,000–2,500	> 1,500	< 150	-6	< 135.0	< 180.0

[1] AASHTO or TX-DOT standards for samples containing more or less than 25% passing the 2 mm (#10) sieve, respectively.

Table 11. Characterization of Corrosivity Scores

Score	GN	Resistivity,[1] Ω.cm	pH[1]	Sulfate,[1] mg/kg	Chloride,[1] mg/kg
0	<3	> 25,000	> 6	< 500	< 150
-1	3–4	2,500–25,000	< 6	500–1,500	> 150
-2	>4	1,000–2,500		> 1,500	
-3		< 1,000			

[1] AASHTO or TX-DOT standards for samples containing more or less than 25% passing the 2 mm (#10) sieve, respectively.

5. Conclusions

This research investigated the electrochemical properties of eight sources of expanded shale, clay, and slate lightweight aggregates. Samples included a combination of fine- and coarse-blended aggregates compared with fine and coarse normal-weight aggregate samples. We characterized each sample based on measurements of gradations, densities, and water absorption following ASTM standards. Electrochemical and geochemical tests included electrical resistivity, pH, and sulfate and chloride ion contents of aggregates in various moisture conditions according to AASHTO, TxDOT, and ASTM, following the criteria described by NASEM (2021). These tests were partially verified through third-party testing by a certified laboratory. Further, corrosion studies were conducted on aggregate samples during wetting, saturation, drainage, and air-drying cycles for 7, 14, 28, 90, 182, and 364 days. Corrosion investigations involved corrosivity rate measurements of galvanized and carbon steel coupons, and comparisons with the electrical resistivity of the aggregates within the soil box and electrical resistivity, pH, sulfate, and chloride ions of aqueous contents.

Lightweight aggregates have 20% to 40% lower density and 500% to 600% higher water absorption than normal weight aggregates. Typical geotechnical blends from lightweight aggregate sources consist of coarse aggregates and lack adequate fines to be tested per AASHTO standards, and therefore justify the application of TxDOT, ASTM, and other standards fitting coarse samples.

Electrochemical and geotechnical test results indicated a significant gap between the properties of coarse and fine aggregates, and, therefore, showed that TxDOT standards were better suited for coarse-blended aggregate application as geotechnical fills. Coarse aggregates have a higher resistivity compared to fine aggregates by a factor of up to 10 for the same sources of materials. Further, the drained condition of materials also increased the resistivity by a factor of 10. Drained aggregates exhibit up to nearly 13 times higher electrical resistivity values compared to wet aggregates. This difference is higher for coarse aggregates than for fine aggregates.

The change in the testing method from AASHTO T 288 to TX-129-M, removing the standing time, increases the recorded electrical resistivity for the same coarse aggregate size. The 24-hour saturation practice in the corrosion tests shows some reduction as conductive contents find adequate time to disperse through the aqueous content.

Comparing pH values obtained from AASHTO T 289 and TX-620-M standards reveals that the testing method has an impact of approximately 2.1% on the measurements, but the difference for individual samples varies between 0.2 and 1.4, for which the latter difference is significant. Similar observations apply to results via ASTM D4972 with an overall 2.4% difference and the individual pH gap between 0.1 and 0.4, with one exception with a difference of 0.7. Data from this study also suggests that electrical resistivity tends to drop as the pH increases, but the low fidelity of suggested curves rejects a strong influence of pH on electrical resistivity.

All observed trends suggest a reduced electrical resistivity for high sulfate and chloride content values. The declining trends of resistivity versus sulfate have a higher coefficient of determination than those for chloride, most likely due to high sulfate concentrations as opposed to chloride contents. With respect to chemical activity, sulfate contents vary between 0.56 and 37 mEq/kg (SO_4^{--} with a valence of 2 mEq/mmole and weight of 96 mg/mmole), and chloride contents vary between 0.021 and 4.6 mEq/kg (Cl^- with a valence of 1 mEq/mmole and weight of 35.5 mg/mmole).

Results indicate that all coarse lightweight aggregate samples have lower corrosion rates than the coarse normal-weight aggregate samples. Further, the average corrosion rate from moist samples is considerably lower than that of wet samples. The difference is larger for coarse blends compared to fine samples, as fine samples keep more moisture after drainage and during air drying.

The saturation process does not significantly affect the corrosion rate, but draining the sample reduces the corrosion rate by one to two orders of magnitude. Further, corrosion rates after rewetting are typically smaller than the initial values. The initial corrosion rate for carbon steel coupons is nearly 25% more than for galvanized steel coupons. Comparing the same rate for the total estimated corrosion over the observed period indicates a 35% higher rate for carbon compared to galvanized steel.

Each wetting and drying cycle results in higher resistivity, lower sulfate and chloride ion contents, and lower corrosion rates, with some exceptions. Cycles of wetting and drying do not appear to influence measurements of pH. Notably, the normal-weight sample has lower sulfate and chloride ion contents than most lightweight aggregates, which confirms prior observations of higher electrical resistivity.

Corrosion tests revealed that the corrosivity of galvanized and carbon steel coupons in lightweight fills does not exceed those of normal-weight aggregates despite having lower resistivity or higher sulfate contents. Hence, guidelines to predict the corrosion rate of lightweight aggregates required revised limits for various electrochemical properties. The thresholds of sulfate and chloride contents before they have a significant effect on corrosion are 200 and 100 mg/kg, respectively. However, the low corrosivity of some samples does not support the adoption of these triggering values for ESCS fills. Thus, it may be appropriate to raise these thresholds to 500 mg/kg for sulfate and 150 mg/kg for chlorides considering the performance of ESCS aggregates.

The outcomes of this study highlight the contribution of expanded shale, clay, and slate lightweight aggregates to the durability of MSE bridge abutments through reduced corrosion. This contribution extends the service life of bridge infrastructure and reduces the lifecycle cost and footprints of the transportation network system.

Bibliography

Standards

AASHTO T 288–12. Standard method of test for determining minimum laboratory *resistivity*. Washington, DC: American Association of State Highway and Transportation Officials.

AASHTO T 289–22. *Standard Method of Test for Determining pH of Soil for Use in Corrosion Testing*. Washington, DC: American Association of State Highway and Transportation Officials.

AASHTO T 290–03. *Standard Method of Test for Determining Water-Soluble Sulfate Ion Content in Soil*. Washington, DC: American Association of State Highway and Transportation Officials.

AASHTO T 291–22. *Standard Method of Test for Determining Water-Soluble Chloride Ion Content in Soil*. Washington, DC: American Association of State Highway and Transportation Officials.

ASTM C127–15. Standard Test Method for Relative Density (Specific Gravity) and Absorption of Coarse Aggregate. West Conshohocken, PA: ASTM International.

ASTM C128–15. Standard Test Method for Relative Density (Specific Gravity) and Absorption of Fine Aggregate. West Conshohocken, PA: ASTM International.

ASTM C136–06. Standard Test Method for Sieve Analysis of Fine and Coarse Aggregates. West Conshohocken, PA: ASTM International.

ASTM C29/C29M-97. Standard Test Method for Bulk Density ("Unit Weight") and Voids in Aggregate. West Conshohocken, PA: ASTM International.

ASTM C33/C33M-18. Standard Specification for Concrete Aggregates. West Conshohocken, PA: ASTM International.

ASTM C330/C330M-14. Standard Specification for Lightweight Aggregates for Structural Concrete. West Conshohocken, PA: ASTM International.

ASTM D4972–19. Standard Test Methods for pH of Soils. West Conshohocken, PA: ASTM International.

ASTM D8262–22. Standard Test Method for Determining the pH of Granular Material for Use in Embankments, Subgrades, and Retaining Wall Backfill. West Conshohocken, PA: ASTM International.

ASTM E11–20. Standard Specification for Woven Wire Test Sieve Cloth and Test Sieves. West Conshohocken, PA: ASTM International.

ASTM G1–03. Standard Practice for Preparing, Cleaning, and Evaluating Corrosion Test Specimens. West Conshohocken, PA: ASTM International.

ASTM G162–18. Standard Practice for Conducting and Evaluating Laboratory Corrosion Tests in Soils. West Conshohocken, PA: ASTM International.

ASTM G187–18. Standard Test Method for Measurement of Soil Resistivity Using the Two-Electrode Soil Box Method. West Conshohocken, PA: ASTM International.

California Test 417. Method of Testing Soils, Concrete Patching Materials and Waters for Sulfate Content. Sacramento, CA: California Department of Transportation.

California Test 422. Method of Testing Soils, Concrete Patching Materials and Waters for Chloride Content. Sacramento, CA: California Department of Transportation.

California Test 643. Method of Test for Laboratory Resistivity and pH for Soil and Water. Sacramento, CA: California Department of Transportation.

TxDOT. Tex-129-M Measuring the Resistivity of Soil Materials. Texas Department of Transportation.

TxDOT. Tex-620-M Determining pH and Chloride and Sulfate Content in Soils. Texas Department of Transportation.

Authored References

AASHTO (American Association of State Highway and Transportation Officials). 2017. LRFD Bridge design specifications. (8th ed). Washington, DC: AASHTO.

Adkins, G., and Rutkowski, N. (1997). Resistivity field testing of mechanically stabilized structures. In 48th *Highway Geology Symposium Proceedings and Fieldtrip Excursion Guide*. Tennessee Department of Transportation, University of Tennessee, Transportation Research Board.

Anderson, P.L., Gladstone, R.A., and Sankey, J.E. (2012). State of the practice of MSE wall design for highway structures. In *Geotechnical Engineering State of the Art and Practice: Keynote Lectures from GeoCongress 2012*, 443–463. https://doi.org/10.1061/9780784412138.0018.

Arciniega, J.L., Walker, W.S., Nazarian, S., and Fishman, K.L. (2019). A model for estimating resistivity of in-service backfill of mechanically stabilized earth walls based on minimum

resistivity and degree of saturation. *Transportation Research Record* 2673(2), 502–508. https://doi.org/10.1177/0361198118825121.

Arciniega, J.L., Walker, W.S., Nazarian, S., and Fishman, K.L. (2018). A process for optimizing gradation of marginal backfill of mechanically stabilized earth walls to achieve acceptable resistivity. *Transportation Research Record*, 2672(52), 251–257. https://doi.org/10.1177/0361198118770166.

Asgari, H., Toroghinejad, M.R., and Golozar, M.A. (2009). Effect of coating thickness on modifying the texture and corrosion performance of hot-dip galvanized coatings. *Current Applied Physics* 9(1), 59–66. https://doi.org/10.1016/j.cap.2007.10.090.

Azoor, R.M., Deo, R.N., Birbilis, N., and Kodikara, J. (2019). On the optimum soil moisture for underground corrosion in different soil types. *Corrosion Science* 159, 108116. https://doi.org/10.1016/j.corsci.2019.108116.

Beben, D. (2015). Backfill corrosivity around corrugated steel plate culverts. *Journal of Performance of Constructed Facilities* 29(6), 04014159. https://doi.org/10.1061/(ASCE)CF.1943-5509.0000654.

Bertolini, L., Elsener, B., Pedeferri, P., Redaelli, E., and Polder, R.B. (2013). *Corrosion of steel in concrete: prevention, diagnosis, repair*. John Wiley and Sons.

Blitz, J., and Simpson, G. (1996). *Ultrasonic methods of non-destructive testing*. London, UK: Chapman and Hall.

Brady, Z., Parsons, R., and Han, J. (2016). Testing Aggregate Backfill for Corrosion Potential. (Report No. T-TRAN: KU-15–5). Lawrence, KS: Kansas Department of Transportation, College of Engineering, University of Kansas. https://rosap.ntl.bts.gov/view/dot/39914.

Broomfield, J. (2003). *Corrosion of steel in concrete: understanding, investigation and repair*. CRC Press. https://doi.org/10.1201/9781482265491.

Castillo, C., Hinojos, J., Bronson, A., Nazarian, S., and Borrok, D.M. (2014). Relating corrosion of mechanically stabilized earth reinforcements with fluid conductivity of backfill soils. (No. 14–3204). In *TRB 93rd Annual Meeting Compendium of Papers*. Washington, DC: Transportation Research Board.

Chen, J., Bronson, A., and Knittel, D.R. (1985). Pitting Corrosion on Zirconium in KCl and KCl-H_2SO_4 Solutions. *Corrosion* 41(8), 438–445. https://doi.org/10.5006/1.3583824.

Darbin, M., Jailloux, J.M., and Montuelle, J. (1988). Durability of Reinforced Earth Structures: The Results of a Long-Term Study Conducted on Galvanized Steel. *Proceedings of the Institution of Civil Engineers* 84(5), 1029–1057. https://doi.org/10.1680/iicep.1988.508.

Darwin, D., Mindess, S., and Young, J.F. 2003. *Concrete.* (2nd ed.). Upper Saddle River, NJ: Prentice-Hall.

Davis, J.R. (2000). *Corrosion: Understanding the basics.* Materials Park, Ohio: ASM International.

Elias, V. (1990). Durability/Corrosion of Soil Reinforced Structures. (No. FHWARD-89–186). McLean, VA: Office of Engineering and Highway Operations.

Elias, V., Fishman, K., Christopher, B.R., Berg, R.R., and Berg, R.R. (2009). Corrosion/degradation of soil reinforcements for mechanically stabilized earth walls and reinforced soil slopes. (No. FHWA-NHI-09–087). Washington, DC: National Highway Institute. https://rosap.ntl.bts.gov/view/dot/39218.

Fontana, M.G., and Greene, N.D. (2018). *Corrosion engineering.* McGraw-Hill.

Harpstead, D.L., Schmidt, J.M. and Christopher, B.R. (2010). Applying lessons learned in the past 20 years of MSE wall design and construction. In *Earth Retention Conference 3,* 478–485. https://doi.org/10.1061/41128(384)47.

Holm, T. A., and Ries, J. P. (2007). *Reference Manual for the Properties and Applications of Expanded Shale, Clay and Slate Lightweight Aggregate.* 2nd edition. Chicago, IL: Expanded Shale, Clay, and Slate Institute. https://www.escsi.org/reference-manual/

Holz, R.D., Christopher, B.R., and Berg, R.R. (1998). Geosynthetic design and construction guidelines. (No. FHWA HI-95–038). Washington, DC: Federal Highway Administration.

IDOT (Illinois Department of Transportation). (2021). *Manual of Test Procedures for Materials.* Springfield, IL: Illinois Department of Transportation.

Jack, T.R., and Wilmott, M.J. (2011). Corrosion by soils. In Revie, R. W. (Ed.), *Uhlig's Corrosion Handbook.* (3rd ed.), 333–349. Hoboken, NJ: John Wiley and Sons.

Johnson, C.M., and Nishita, H. (1952). Microestimation of sulfur in plant materials, soils, and irrigation waters. *Analytical chemistry* 24(4), 736–742. https://doi.org/10.1021/ac60064a032.

Jones, D.A. (1996). *Principles and prevention of Corrosion.* (2nd ed.). Upper Saddle River, NJ: Prentice Hall.

Knittel, D.R., and Bronson, A. (1984). Pitting corrosion on Zirconium—a review. *Corrosion* 40(1), 9–14. https://doi.org/10.5006/1.3579296.

Kolay, P.K., Tajhya, D., and Mondal, K. (2020). Corrosion of steel in MSE walls due to deicers and backfill aggregates. *Geotech Geol Eng* 38, 2493–2507. https://doi.org/10.1007/s10706-019-01164-w.

Marot, D., Bendahmane, F., and Nguyen, H.H. (2012). Influence of angularity of coarse fraction grains on internal erosion process. *La Houille Blanche* (6), 47–53. https://doi.org/10.1051/lhb/2012040.

McCarter, W.J. (1984). The electrical resistivity characteristics of compacted clays. *Geotechnique* 34(2), 263–267. https://doi.org/10.1680/geot.1984.34.2.263.

Munjy, H., Tehrani, F., Xiao, M., and Zoghi, M. (2014). A Numerical Simulation on the Dynamic Response of MSE Wall with LWA Backfill. In Hicks, M.A., Brinkgreve, R.B.J., and Rohe, A. (Eds.) *Proc. Numerical Methods in Geotechnical Engineering* Vol. 1, CRC Press, Taylor and Francis Group: London, UK, 1147–1152. www.crcpress.com/Numerical-Methods-in-Geotechnical-Engineering/Hicks-Brinkgreve-Rohe/p/book/9781138001466.

NASEM (National Academies of Sciences, Engineering, and Medicine). (2011). *LRFD Metal Loss and Service-Life Strength Reduction Factors for Metal-Reinforced Systems*. Washington, DC: The National Academies Press. https://doi.org/10.17226/14497.

NASEM (National Academies of Sciences, Engineering, and Medicine). (2020). *Improved test methods and practices for characterizing steel corrosion potential of earthen materials*. (No. NCHRP Project 21–11). Washington, DC: The National Academic Press (NAP). https://doi.org/10.17226/25925.

NASEM (The National Academies of Sciences, Engineering, and Medicine). (2021). *Electrochemical Test Methods to Evaluate the Corrosion Potential of Earthen Materials*. Washington, DC: The National Academies Press (NAP). https://doi.org/10.17226/26076.

NCHRP (National Cooperative Highway Research Program). (1978). Durability of Drainage Pipe. (NCHRP 50). Washington, DC: Transportation Research Board.

Padilla, V., and Alfantazi, A. (2013). Corrosion performance of galvanized steel in Na_2SO_4 and NaCl solutions at subfreezing temperatures. *Corrosion* 69(2), 174–185. https://doi.org/10.5006/0645.

Padilla, V., Ghods, P., and Alfantazi, A. (2013). Effect of de-icing salts on the corrosion performance of galvanized steel in sulphate contaminated soil. *Construction and Building Materials* 40, 908–918. https://doi.org/10.1016/j.conbuildmat.2012.09.077.

Petrasic, K. (2008). MSE Wall Backfill Testing: Sample Preparation for Accurate Modeling. NESMEA, Atlantic City, NJ: Pennsylvania Department of Transportation.

Porter, F.C. (1994). *Corrosion resistance of zinc and zinc alloys*. CRC Press. https://doi.org/10.1201/9781482293524.

Revie, R.W. (2008). Corrosion and corrosion control: an introduction to corrosion science and engineering. John Wiley and Sons.

RILEM Technical Committee (Masayasu Ohtsu). (2010). Recommendation of RILEM TC 212-ACD: acoustic emission and related NDE techniques for crack detection and damage evaluation in concrete. *Mater Struct* 43, 1183–1186. https://doi.org/10.1617/s11527–010–9639-z.

Sadrinezhad, A., Tehrani, F.M., and Jeevanlal, B. (2019). Shake Table Test of Railway Embankment Consisting of LWA and TDA. In Meehan, C.L., Kumar, S., Pando, M.A., and Coe, J.T. (Eds.). *Proc. 8th International Conference on Case Histories in Geotechnical Engineering*, Philadelphia, PA: ASCE, March 2019, 31–39. https://ascelibrary.org/doi/10.1061/9780784482100.004.

Salazar, M. (2010). Nevada DOT's Experience with MSE Wall Corrosion. The 35th Southwest Geotechnical Engineers Conference, Nevada Department of Transportation.

Samouëlian, A., Cousin, I., Tabbagh, A., Bruand, A., and Richard, G. (2005). Electrical resistivity survey in soil science: a review. *Soil and Tillage Research* 83(2), 173–193. https://doi.org/10.1016/j.still.2004.10.004.

Snapp, M.A. (2015). *Electrical Resistivity Measurements of Mechanically Stabilized Earth Retaining Wall Backfill*. (MSc Thesis), Kansas State University. http://hdl.handle.net/2097/19771.

Stott, J.F.D., and John, G. (2010). Corrosion in Soils. In Cottis, B., Graham, M., Lindsay, R., Lyon, S., Richardson, T., Scantlebury, D., and Stott, H. (Eds.). *Shreir's Corrosion* 2, 1149–1168. https://doi.org/10.1016/B978-044452787-5.00047-0.

Szklarska-Smialowska, Z. (1986). *Pitting corrosion of metals*. Houston, TX: National Association of Corrosion Engineers.

Tehrani, F. M. (1998). Rāhnamā-ye Jāme'-e Līkā. [Leca Handbook, in Persian]. Tehran, Iran: Leca Co. https://leca.ir/wp-content/uploads/maghalat/LECA-Handbook.pdf

Tehrani, F.M. (2021). Non-Corrosivity of Expanded Shale, Clay and Slate Aggregate in Mechanically Stabilized Earth Fills, ESCSI E-Newsletter, Summer 2021.

Tehrani, F. M. (2022). Deployment of Sustainable Practices using Lightweight Aggregates for Bridge Infrastructures. In Davis, C. A., Yu, K., and Taciroglu, E. (eds.), *Proc. ASCE Lifelines 2022: 1971 San Fernando Earthquake and Lifeline Infrastructure*, Los Angeles, CA: University of California, Los Angeles. (February 7-11, 2022): 187-197. https://doi.org/10.1061/9780784484432.018.

Tehrani, F. M. (2023a). Sustainability from The Ground Up. *Civil + Structural Engineer*, April 1, 2023, 9(4): 12-13. https://csengineermag.com/sustainability-from-the-ground-up/.

Tehrani, F. M. (2023b). Application of Environmental Product Declarations in Sustainability of Geotechnical Structures. In Rathje, E., Montoya, B. M., and Wayne, M. H. (eds.), *Proc. ASCE Geo-Congress 2023, GSP 339: Soil Improvement, Geoenvironmental, and Sustainability*, Los Angeles, CA. (March 26-29, 2023): 661-670. https://doi.org/10.1061/9780784484661.069

Tehrani, F.M., Tizhoosh, F.T., Mousavi, S.M., and Kavand, A. (2018). An Experimental Investigation of a Full-scale Reinforced Lightweight Aggregate Embankment. *Advance Researches in Civil Engineering* 1(2), 36–41. https://dx.doi.org/10.30469/arce.2019.85700.

Tehrani, F. M., M. Zoghi, and M. Xiao. (2016). A Numerical Simulation of Mechanically Stabilized Walls. In *Proc. 5th International Conference on Geotechnical Engineering and Soil Mechanics*, Tehran, Iran: IGS. (November 2016): 671. www.issmge.org/events/5th-international-conference-on-geotechnical-engineering-and-soil-mechanics

Thapalia, A., Borrok, D.M., Nazarian, S., and Garibay, J. (2011). Assessment of corrosion potential of coarse backfill aggregates for mechanically stabilized earth walls. *Transportation research record* 2253(1), 63–72. https://doi.org/10.3141/2253-07.

Vilda III, W.S., Lindemuth, D., Ellor, J.A., Islam, M., Ault, J.P., Flounders Jr, E.C. and Repp, J., (2009). Corrosion in the soil Environment: Soil Resistivity and PH Measurements. National Cooperative Highway Research Program (NCHRP).

Xiao, M., Tehrani, F., and Zoghi, M. (2013). Seismic Responses of MSE Walls Using Accelerated Alternative Backfill Materials with Recycled Tires Shreds and Lightweight Expanded Aggregates. (Report No. CA13–2416). Sacramento, CA: CA Department of Transportation. https://trid.trb.org/view/1290312.

Zaki, A., Chai, H.K., Aggelis, D.G., and Alver, N. (2015). Non-destructive evaluation for corrosion monitoring in concrete: A review and capability of acoustic emission technique. *Sensors* 15(8), 19069–19101. https://doi.org/10.3390/s150819069.

About the Authors

Prof. Dr. Fariborz M. Tehrani, PhD, PE, ENV SP, PMP, SAP, F.ASCE

Dr. Fariborz M. Tehrani is a Professor and Director with more than three decades of academic and industry background in engineering design, management, education, and leadership. His research and practice experiences focus on sustainable and resilient structural engineering, mechanics, and materials (SR-SEMM). Fariborz is a Fellow ASCE, the Director of the ESCSI, a voting member of several ACI, ASTM, and TRB Committees, the EMI's Liaison in the ASCE Sustainability Task Committee, and the Vice Chair of EMI Objective Resilience Committee. He has also served as the ISI Academic Committee Chair and EWB professional mentor in USC, UCSD, and Cal Poly SLO. He has over 100 published and over 110 presented scholarly works. Dr. Tehrani received the 2015 ASCE Region 9 Outstanding Faculty Advisor Award, the 2017 CHESC Best Practice Award, and two 2019 ASCE Research Awards from Fresno and San Francisco for two projects. He received his BSc from Sharif University of Technology, his MSc from Amirkabir University of Technology, and his MS, Degree of Engineering, and PhD from the University of California, Los Angeles.

Dr. Kenneth L. Fishman, PhD, PE, M.ASCE

Dr. Kenneth L. Fishman, PhD, PE is a geotechnical engineer and principal at McMahon and Mann Consulting Engineering and Geology, P.C. where he leads the Earth Reinforcement Testing Division. For the past 25 years, he has been involved in the research and application of corrosion testing and corrosion mitigation for buried steel. He has served on numerous projects related to condition assessment, corrosion monitoring, and expected service life modeling for earth reinforcements. These projects include research, the implementation of research results, training, and applications of state-of-the-art techniques for performance monitoring and the characterization of corrosion potential. They have involved different transportation agencies, suppliers of earth reinforcement systems, dam owners, mine operators, railway operators, contractors, and engineering consultants scattered throughout North America. Dr. Fishman served as PI for NCHRP Project 21-11 "Improved Test Methods and Practices for Characterizing Steel Corrosion Potential of Earthen Materials," and was appointed to the National Academy of Science Engineering and Medicine (NASEM) ad hoc Committee on "The Corrosion of Buried Steel at New and In Service Infrastructure." He has participated in numerous workshops and webinars sponsored by NCHRP, FHWA, AASHTO, TRB and others including two webinars related to asset management and performance modeling sponsored by the FHWA Office of Asset Management and Resource Center, AASHTO, and TRB. Dr. Fishman has extensive experience reviewing technical documents having served as an editor for the ASCE *Journal of Geotechnical and Geoenvironmental Engineering*, and current assignments as an editor for *Geostrata*, and member of the ASCE Geo-Institute (GI) Technical Publications Committee with responsibilities including editing for the ASCE series on Geotechnical Practice Publications (GPP).

Mr. Farmehr M. Dehkordi, MSc, M.RILEM

Mr. Farmehr M. Dehkordi is a Rilem member and Ph.D. student in Civil and Environmental Engineering at Politecnico di Torino and a visiting research assistant at California State University, Fresno. His research interests include the application of fiber-reinforced brittle materials, such as fiber-reinforced concrete (FRC) and fiber-reinforced ice (FRI). He received his BSc from Isfahan University of Technology and his MSc from Politecnico di Torino.